UC San Diego
UC San Diego Previously Published Works

Title

Probing neutrino physics with a self-consistent treatment of the weak decoupling, nucleosynthesis, and photon decoupling epochs

Permalink

https://escholarship.org/uc/item/06p9k442

Journal

Journal of Cosmology and Astroparticle Physics, 2015(05)

ISSN

1475-7516

Authors

Grohs, E
Fuller, George M
Kishimoto, Chad T
et al.

Publication Date

2015-05-01

DOI

10.1088/1475-7516/2015/05/017

Peer reviewed

You may also be interested in:

Probing neutrino physics with a self-consistent treatment of the weak decoupling, nucleosynthesis, and photon decoupling epochs

E. Grohs,[a,1] **George M. Fuller,**[a] **Chad T. Kishimoto**[a,b] **and Mark W. Paris**[c]

[a]Department of Physics, University of California,
  San Diego, La Jolla, California 92093-0319, U.S.A.

[b]Department of Physics, University of San Diego,
  San Diego, California 92110, U.S.A.

[c]T-2 Nuclear & Particle Physics, Astrophysics & Cosmology, Theoretical Division,
  Los Alamos National Laboratory, Los Alamos, New Mexico 87545, U.S.A.

E-mail: egrohs@physics.ucsd.edu, gfuller@ucsd.edu, ckishimo@physics.ucsd.edu,
  mparis@lanl.gov

Abstract. We show that a self-consistent and coupled treatment of the weak decoupling, big bang nucleosynthesis, and photon decoupling epochs can be used to provide new insights and constraints on neutrino sector physics from high-precision measurements of light element abundances and Cosmic Microwave Background observables. Implications of beyond-standard-model physics in cosmology, especially within the neutrino sector, are assessed by comparing predictions against five observables: the baryon energy density, helium abundance, deuterium abundance, effective number of neutrinos, and sum of the light neutrino mass eigenstates. We give examples for constraints on dark radiation, neutrino rest mass, lepton numbers, and scenarios for light and heavy sterile neutrinos.

---

[1]Corresponding author.

Contents

1 Introduction

In this paper we demonstrate how a self-consistent treatment of the physics of the early universe (from temperature $T \sim 10\,\text{MeV}$ down to $T \sim 0.1\,\text{eV}$) enables Cosmic Microwave Background (CMB) observations, in concert with light-element abundances, to be used as new probes of beyond-standard-model (BSM) physics in the neutrino sector. In a sense, these probes are tantamount to probes of the CνB (relic Cosmic Neutrino Background). Recent observations [1–4] of the CMB and observationally-inferred primordial abundances of deuterium and helium [5–8] formed in big bang nucleosynthesis (BBN) already place tight constraints on both the cosmological standard model (CSM) and BSM physics. However, future observations will usher in a higher level of precision with even better prospects for BSM probes, see for example ref. [9].

We anticipate that observations will bring about an overdetermined situation where BSM physics may manifest itself if it is present. The existing or anticipated observations and measurements of greatest utility for the present purposes are: (1) high-precision measurements of the baryon-to-photon ratio, or the equivalent baryon density ($\omega_b \equiv \Omega_b h^2$); (2) high-precision measurements of the "effective number of relativistic degrees of freedom" (N_{eff}); (3) high-precision measurements of the primordial deuterium abundance (D/H) from quasar absorption lines; (4) measurements of the primordial helium abundance (Y_P) directly from CMB polarization data; and (5) measurements of the sum of the light neutrino masses ($\sum m_\nu$), i.e. the collisionless damping scale associated with neutrinos.

The physics that determines the relic neutrino energy spectra in weak decoupling and that of primordial nucleosynthesis affects observables of the CMB. These distinct, disparate epochs, however, depend not only on the values of parameters describing the cosmology (such as ω_b, $N_{\rm eff}$, relevant cosmic constituents, etc.) but also on the parameters derived from these base, input parameters (such as primordial abundances, recombination history, etc.). This is the basis for what we will term "self-consistency." The requirement for self-consistency between the BBN and CMB epochs, for example, in current data analyses depends on the parametrization of the energy density in terms of $N_{\rm eff}$ and upon the baryon-to-photon ratio. These two parameters, as measured at photon decoupling, are the sole determinants of the primordial helium abundance at the epoch of alpha particle formation ($T \sim 0.1\,{\rm MeV}$) in "standard" (i.e. zero lepton numbers, no BSM physics) BBN calculations. Though this procedure is adequate for the CSM and standard model physics, here we argue that it can be insufficient to probe varieties of BSM physics when confronting model cosmologies with next-generation, high-precision CMB and light element abundance data. In the case of the helium and $N_{\rm eff}$ self-consistency mentioned above, the relationship between the helium yield in BBN and $N_{\rm eff}$ is a non-trivial function of the interplay of expansion rate and neutron-to-proton ratio, as is well known [10]. The latter ratio is, in turn, a sensitive function of the ν_e and $\bar{\nu}_e$ energy distribution functions, and these can be affected by BSM issues like lepton numbers, flavor mixing, sterile neutrino states, heavy particle decay, etc.

Handling and analyzing the observed data while imposing self-consistency over multiple epochs in the early universe can require new procedures. The approach developed in ref. [10] and employed in Planck XVI [11] has been highly successful. There, self-consistency is imposed approximately by the addition of a term in the log-likelihood function. A very small theoretical uncertainty ensures the posterior distributions are close to the corresponding theoretical values. However, when we impose self-consistency among the different epochs the need may arise to solve for the various derived parameters iteratively. Returning to the helium/$N_{\rm eff}$ example discussed above, Y_P and the recombination history of the universe both depend on the radiation energy density, usually parametrized by $N_{\rm eff}$. Subsequently, the recombination history is affected by the the primordial abundance of helium. The values of these two derived parameters, in turn, affect CMB observables, which recommends an iterative and therefore self-consistent approach.

Ideally, we would want a procedure to self-consistently treat neutrino and BSM physics from the post-QCD epoch to the onset of non-linearities in large scale structure (LSS). Recently, the quantum-kinetic equations (QKEs) governing neutrino flavor evolution in dense environments have been derived from first principles [12–14]. Such a program to treat neutrino physics in the early universe would incorporate a QKE treatment through weak decoupling at the very least. Weak freeze-out and BBN necessitate a neutrino-energy Boltzmann-equation or QKE treatment fully coupled to a nuclear reaction network. The recombination, photon decoupling, and advent of LSS epochs require a Boltzmann-equation treatment of neutrino clustering. Verification of any models related to neutrinos and BSM physics would then rely on agreement with direct cosmological observables, including but not limited to: primordial abundances; CMB power spectra; and the total matter power spectrum.

As outlined, this is a challenging undertaking. We therefore employ a limited approach to show why self-consistency is required and how such a treatment can be efficacious in probing some issues in neutrino sector physics. To that end, we calculate the ratio of sound horizon to photon diffusion length, r_s/r_d, as a simple parametrization of the CMB, as described in detail in section 3. It would, of course, be preferable to compute the full CMB

power spectra in the self-consistent manner described above. There are two limiting factors that temper this ambitious proposal, however. The first is that the observable r_s/r_d is largely insensitive to the poorly constrained equation of state of the dark, vacuum energy component while the CMB power spectra are not. Additionally, current computations of the CMB power spectra [15] would need to be generalized to the BSM scenarios we contemplate here.

Our procedure for calculating derived cosmological quantities utilizes the neutrino occupation probabilities. Since we are developing the capacity to compute the effects of BSM physics that couples to the active neutrino sector, we do not restrict the form of the neutrino distribution functions to that of equilibrium Fermi-Dirac distributions. General forms are permitted and may be handled analytically or numerically. Neutrino occupation probabilities are taken in the present work in the flavor eigenbasis during weak decoupling, weak freeze-out and BBN.[1] During recombination and last scattering, we transform the occupation probabilities to the mass eigenbasis. When we consider the case of massive neutrinos, the statistic for the sum of the light neutrino masses, $\sum m_\nu$, is simply the sum of the three lightest mass eigenstates.

We might further clarify the fact that this limited approach does not rely on the assumption that the radiation energy density can be described in terms of the single parameter $N_{\rm eff}$. Indeed, an original motivation for using r_s/r_d as a proxy for $N_{\rm eff}$ (see section 3) is the fact that the usual definition for $N_{\rm eff}$ does not apply to non-equilibrium neutrino distributions. A corollary of this observation is the possibility that $N_{\rm eff}$ may depend on the scale factor $a(t)$; that is, we do not assume that $N_{\rm eff}$ is independent of scale factor. When extended, our approach is able to handle BSM scenarios such as the decay of massive sterile neutrinos and other weakly interacting massive particles, which result in neutrino distributions that may differ substantially from a Fermi-Dirac distribution [16].

Our approach aims to be general; it does not rely on particular cosmological models but is appropriate to the class of Λ cold-dark matter (ΛCDM) models. It extends and explicates recent work [9, 10, 17, 18] on the consistent incorporation of precision observations of the CMB [11] and observations of the light element abundances of helium and deuterium (mass fraction Y_P and relative abundance D/H). The deuterium abundance [6, 8] is now more precisely measured by a significant factor (4 or 5) in relative precision than Y_P. Our results indicate that deuterium is sufficiently well determined to be incorporated into CSM analyses as a fixed prior.

The present work is a first result in an ongoing campaign to incorporate neutrino energy transport into a self-consistent treatment of BBN and recombination. Our approach is being implemented in FORTRAN90/95 as a suite of codes under the working title of "BBN Unitary Recombination Self-consistent Transport" (BURST), which will be made publicly available for use on parallel computing platforms using OPENMPI. The current work is a prerequisite in an ongoing collaboration to develop codes that consistently handle BBN and neutrino energy transport from weak decoupling to the advent of LSS.

The paper is outlined as follows. In the following section, section 2, we discuss our treatment of BBN and relevant CMB physics. Section 3 explains the self-consistent, iterative approach to determining $N_{\rm eff}$ using r_s/r_d. Section 4 employs a dark-radiation model to test the accuracy of predictions made by BURST against observations. Section 5 investigates a number of 'test problems' from BSM physics suited for BURST. We conclude in section 6 with future applications of the results given in this work. Throughout this paper, we use natural units where $\hbar = c = k_B = 1$.

---

[1]This is a matter that is properly resolved by utilizing a QKE approach [12], the subject of a future study.

2 Background

2.1 Big-bang nucleosynthesis

Recently there has been a dramatic increase in precision in the determination of D/H [8]. This improvement in observational precision drives the need to improve the standard tools used to calculate observables during the BBN and CMB epochs. This development allows us to consider improved descriptions of nuclear physics and non-standard particle and cosmological models.

We have developed a generalized BBN subroutine, part of the larger BURST code. The current BBN routine handles general distribution functions for particles out of equilibrium. It numerically integrates the binned neutrino occupation probabilities to obtain thermodynamic variables and number and energy densities for $\nu_e, \bar{\nu}_e, \nu_\mu, \bar{\nu}_\mu, \nu_\tau, \bar{\nu}_\tau$. It is worthwhile, therefore, to summarize our approach to BBN even though it is substantially similar in some respects to that given in refs. [19–21].

We assume that the cosmic fluid is homogeneous and isotropic and that the comoving number density of baryons is covariantly conserved. Neutrinos can experience, in addition to gravity, essentially arbitrary interactions within the Boltzmann transport approximation.[2] We allow for the possibility that neutrinos may decouple from the plasma with non-equilibrium distributions. This assumption implies that there may be deviations from the Fermi-Dirac momentum distribution [22–24]. In fact, it was this observation that provided initial motivation for developing the current approach.

BBN codes evolve light nuclide abundances $Y_i(t)$, defined as

$$Y_i(t) = \frac{n_i(t)}{n_b(t)}, \tag{2.1}$$

as a function of comoving time t in the background of the Friedmann-Lemaître-Robertson-Walker (FLRW) geometry. Here $n_i(t)$ is the proper number density of nuclide $i = n, p, {}^2\text{H}$, ${}^3\text{He}, {}^4\text{He}, \ldots$ and $n_b(t)$ is the proper baryon number density. We will focus on two specific nuclides in this paper: the ${}^4\text{He}$ mass fraction ($Y_P \equiv 4Y_{{}^4He}$), and the ${}^2\text{H}$ relative abundance (D/H $\equiv Y_D/Y_H$). The evolution starts from a time when the plasma temperature T is near $30\,\text{MeV}$. Weak equilibrium obtains at this temperature. The time dependence of the metric is determined by the energy density $\rho(a)$ as

$$H(a) = \frac{\dot{a}}{a} = \sqrt{\frac{8\pi}{3m_{\text{pl}}^2}\rho(a)}, \tag{2.2}$$

where $H(a)$ is the Hubble parameter, m_{pl} is the Planck mass, and the 'dot' indicates differentiation with respect to the FLRW-coordinate time t. The energy density is computed as the integral of the single-particle energy over the momentum distribution:

$$\rho(a) = \sum_j \int \frac{d^3p}{(2\pi)^3} f_j(p; a)\sqrt{p^2 + m_j^2} \tag{2.3}$$

where the sum over j reflects all species contributing to the energy density, including but not limited to: photons, baryons, dark matter, $e^\pm$, and neutrinos. Consistent with the

---

[2]However, the code can handle limited generalizations of the Boltzmann approximation to incorporate effects associated with neutrino quantum kinetics.

above discussion, we do not need to assume a well defined temperature for any of the cosmic species. The time dependence of the distribution function $f_i(p; a)$ is indicated by the presence of the scale factor $a(t)$ in its argument. Evolution in time of the distribution functions is accomplished by solving transport equations, such as the Boltzmann equation, in FLRW geometry.

Given initial conditions for the temperature T and momentum distributions of the cosmological constituents (assumed to be in equilibrium through weak and strong interactions), the BBN code determines the evolution, with respect to the scale factor $a(t)$ (related to time as $dt = da/(aH(a))$), of the temperature of the plasma $T(a)$, the electron chemical potential $\mu_e(a)$, and the nuclide abundances relative to baryon number $Y_i(a)$.

The interactions of the light nuclear species is governed by the nuclear reaction network.[3] The reaction network, which is determined by a chosen set of nuclides and the thermally averaged reactivities $n_{\alpha_1} n_{\alpha_2} \langle \sigma_{\beta\alpha} v_\alpha \rangle$, is proportional to the rate of change of the number density of nuclides participating either in the initial state n_{α_i} or final state n_{β_j} where i, j indexes particles (up to 3) in the initial α or final β channel for the process $\alpha \to \beta$; that is, α and β are two- or three-body reaction channels and α_i is the ith nuclide of the channel α. The nuclear reaction network includes nuclides with mass number $A \leq 9$. Our code allows for the inclusion of additional nuclides with $A > 9$, but we maintain the smaller network as the larger network provides no new insights for this paper. The nuclides are taken to be in thermal equilibrium with the photon-electron plasma. We are currently employing an updated [25] version of the reaction network from ref. [21]. We also couple in all relevant $e^\pm$ and neutrino-induced weak interactions (charged and neutral current) [26].

2.2 Cosmic Microwave Background

The physics of BBN and photon decoupling are related through the epoch of recombination by several mechanisms including, importantly, He I and He II recombination. The recombination rates depend sensitively on the amount of ^{4}He created in BBN [10, 27, 28]. The ^{4}He dependence also determines the photon diffusion damping wave number k_d or, equivalently, the photon diffusion length, defined as $r_d \equiv \pi/k_d$. This quantity depends strongly on the recombination history through the free-electron fraction, $X_e(a)$, which, in turn, depends on the helium abundance (see section 2.2.3 below).

We relate the diffusion length directly to an observed angular size θ_d through the angular diameter distance D_A at the epoch of last scattering (as described in detail below). Since D_A depends on the vacuum (dark) energy equation of state, which is poorly understood, we employ the ratio θ_s/θ_d, equivalent to r_s/r_d (see eqs. (2.6) and (2.13)), where θ_s is the angle subtended by the sound horizon, which eliminates explicit dependence on the dark energy equation of state.

Modern computations of the recombination history of the early universe are available in accurate and well tested codes such as HyRec [29], CosmoRec [30], and the fast, approximate computations given in ref. [31] by the code RecFast [32]. Our recombination history compares well with RecFast, agreeing at the level of $< 2\%$ over the recombination epoch. The present accuracy suffices for the purposes of the current exploratory work.

---

[3]The nuclear reaction network should be derived from reaction cross sections that are governed by the principles of quantum mechanics, such as unitarity. We are currently developing a unitary reaction network for application in future work.

2.2.1 Sound horizon

The sound horizon is defined as

$$r_s(a_{\gamma d}) = \int_0^{a_{\gamma d}} da \, \frac{1}{a^2 H(a)\sqrt{3(1+R(a))}} \tag{2.4}$$

where $a_{\gamma d}$ is the scale factor at photon decoupling.[4] The ratio $R(a)$ is given as

$$R(a) = \frac{3\rho_b(a)}{4\rho_\gamma(a)}, \tag{2.5}$$

where ρ_b and ρ_γ are the baryon rest mass and photon field energy densities, respectively.

The angular size of the sound horizon θ_s,[5] determined from the spacing of the acoustic peaks in the CMB temperature power spectrum, is related to the sound horizon by the angular diameter distance $D_A(a_{\gamma d})$ at photon decoupling (scale factor $a_{\gamma d}$) as

$$\theta_s(a_{\gamma d}) = a_{\gamma d} \frac{r_s(a_{\gamma d})}{D_A(a_{\gamma d})}, \tag{2.6}$$

since the angle θ_s is small. The angular diameter distance is

$$D_A(a) = a \int_a^{a_0} da' \left[a'^2 H(a') \right]^{-1}. \tag{2.7}$$

The quantity $D_A(a_{\gamma d})$ depends on the vacuum (dark) energy equation of state, which is not very well understood. Our approach will eliminate dependence on this poorly constrained component of the energy density.

2.2.2 Free-electron fraction

We have written an independent code to calculate the free-electron fraction, X_e. The results agree well with ref. [32] (RecFast). In fact, the agreement is within 2% for most of the range $10^{-4} \lesssim a/a_0 \lesssim 10^{-3}$ ($10^4 \gtrsim z \gtrsim 10^3$). We have not included additional fit parameters, as in ref. [32], that modify recombination and ionization terms of the three-level treatment to obtain agreement with the full 300-level computation [31]. The code allows significant deviations from the model parameters of ΛCDM; it should be used with caution, however, since the effective three-level treatments for helium and hydrogen recombination have been optimized for near-standard model parameters.

The number density of free and total electrons is

$$n_e^{(\text{free})} = n_p + n_{\text{He II}} + 2n_{\text{He III}}, \tag{2.8}$$

$$n_e^{(\text{tot})} = n_b \left(1 - \frac{Y_P}{2} \right), \tag{2.9}$$

where n_b, n_p, $n_{\text{He II}}$, $n_{\text{He III}}$ are the proper number densities for baryons, protons, singly- and doubly-ionized helium, respectively. We write the free-electron fraction as

$$X_e \equiv \frac{n_e^{(\text{free})}}{n_e^{(\text{tot})}} \equiv X_p + X_{\text{He II}} + 2X_{\text{He III}}, \tag{2.10}$$

so defined to take values in the range $0 \leq X_e \leq 1$.

---

[4]Reference [11] takes $a_{\gamma d} \to a_\star$ where the optical depth is unity.

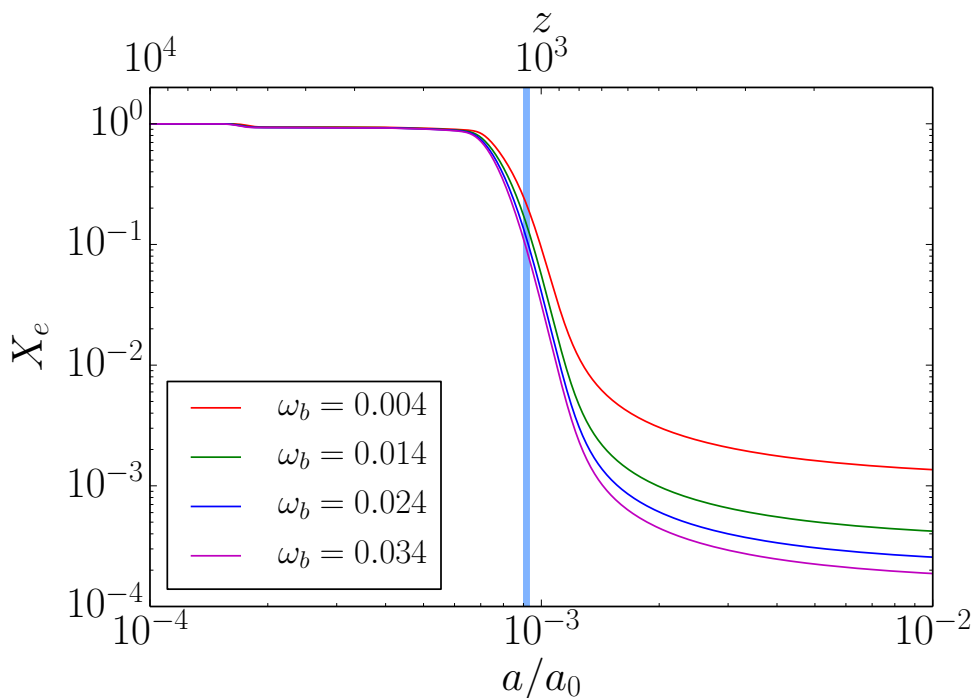[5]Reference [11] takes $\theta_s \to \theta_\star$.

Figure 1. Free-electron fraction X_e as a function of scale factor a/a_0 and redshift z (at top.) The different curves correspond to various values of ω_b. The cold dark matter contribution is held fixed at $\omega_c = 0.12029$. The vertical shaded bar is the scale factor at photon decoupling, $a_{\gamma d}$ given by ref. [11].

We follow refs. [33, 34] and consider the simplification of the multi-level hydrogen and helium atoms to that of an effective three-level system which includes the ground $n = 1$ state, the first excited $n = 2$ states, and the continuum. All other excited states are assumed to be in equilibrium with the $2s$ state. We treat He II recombination approximately [31] (via the Saha equation) since it is essentially complete at the advent of the epoch of He I recombination. The He III contribution, therefore, in the Boltzmann equation for He II is negligible.

Boltzmann equations for H II and He II contain a thermally-averaged cross section and relative velocity $\langle \sigma v \rangle$. We use Case B recombination coefficients for the $\langle \sigma v \rangle$ of both neutral hydrogen [35] and helium [36]. Along with a Saha equation for He III, the Boltzmann equations for H II and He II are a coupled set of ordinary differential equations constituting a recombination network to model the ionization history of the universe prior to photon decoupling.

Fig. 1 shows the evolution of the free-electron fraction with scale factor for various values of ω_b and concomitant values of Y_P. The vertical shaded bar is centered on $a_{\gamma d}$, the scale factor at photon decoupling, given by ref. [11] for a best-fit-value $\omega_b = 0.022068$. The recombination rate increases with increasing ω_b which results in a lower freeze-out value of the free-electron fraction at large a/a_0. The recombination history is largely insensitive to the helium fraction but we calculate Y_P for each value of ω_b to maintain self-consistency between BBN and recombination. The values of Y_P are $Y_P = 0.220, 0.238, 0.243, 0.246$ for increasing ω_b.

2.2.3 Photon diffusion damping length

In the tightly coupled limit, photon diffusion damping is characterized through the damping wave number [37–40]

$$k_d^{-2} = \int_0^{a_{\gamma d}} \frac{da}{a^2 H(a)} \frac{1}{a n_e(a) \sigma_T} \frac{R^2(a) + \frac{16}{15}(1 + R(a))}{6(1 + R(a))^2},$$ (2.11)

where σ_T is the Thomson cross section. Here, we have assumed that moments of the temperature fluctuation higher than the quadrupole make a negligible contribution in the linearized Boltzmann equation for the photon distribution.

Equation (2.11) requires the free-electron fraction, $n_e(a)$, determined in the recombination history, as discussed in the previous section. The free-electron fraction, over the course of the recombination history, depends strongly on the primordial helium mass fraction Y_P. The fraction Y_P, in turn, depends on the relativistic energy density, which is often parametrized in terms of the parameter N_{eff}:

$$\rho_r = 2 \left[1 + \frac{7}{8} \left(\frac{4}{11} \right)^{4/3} N_{\text{eff}} \right] \frac{\pi^2}{30} T^4.$$ (2.12)

Equation (2.12) is only valid after the epoch of $e^{\pm}$ annihilation. The point that BBN and recombination are related is well known [10] but has not been implemented self-consistently as a constraint for general, BSM physics model cosmologies. We return to it after describing the relation between r_s and k_d to directly observable quantities given by the CMB power spectrum.

The observed diffusion angle $\theta_d(a_{\gamma d})$ [11] is related to the diffusion damping length, $r_d = \pi/k_d$ as

$$\theta_d(a_{\gamma d}) = a_{\gamma d} \frac{r_d(a_{\gamma d})}{D_A(a_{\gamma d})},$$ (2.13)

with the same stipulation regarding the smallness of the angle in eq.(2.6).

3 r_s/r_d as a proxy for N_{eff}

In this section we describe our method for determining N_{eff} in detail. We introduce two variants of N_{eff}. When referring to the radiation energy density equation (2.12), which takes as an input the quantity N_{eff}, we designate N_{eff} as $N_{\text{eff}}^{(\text{th})}$. When considering general cosmologies, perhaps with BSM physics, we deduce the value of N_{eff} from the observable quantity $r_s/r_d = \theta_s/\theta_d$, described in this section, and designate it as $\tilde{N}_{\text{eff}}$. The simplest cosmologies for which eq. (2.12) obtains, having negligible neutrino mass, standard model constituents and no energy transfer between species have $N_{\text{eff}}^{(\text{th})} = \tilde{N}_{\text{eff}}$.

We consider a test input cosmology that is non-standard yet substantively similar to ΛCDM. We proceed by determining Y_P at temperature $T \sim 0.1\,\text{MeV}$ using the BBN network of BURST [25]. The principal observational cosmological input at this time is ω_b. Also input and incorporated into the BBN subroutine is any neutrino and BSM physics that constitute the test cosmology. Subsequently, we compute the recombination history of the universe from early times ($a/a_0 \sim 10^{-7}$) to the current epoch. Specific observational inputs include ω_b, ω_c (where for cold dark matter $\omega_c \equiv \Omega_c h^2$), Y_P, and H_0 (the Hubble constant, $H_0 = H(a_0)$).

For the purposes of the present discussion, other inputs of particular importance include neutrino occupation probabilities (as output from a neutrino transport calculation of weak decoupling that is fully coupled to BBN) and neutrino rest masses. The neutrino energy density of the neutrino seas is calculated by writing the occupation probabilities in the mass eigenbasis [41]. We emphasize the fact that $N_{\rm eff}^{\rm (th)}$ is *not* input as a base parameter; this is of paramount import in the present approach. The recombination history, $n_e(a)$ determines the optical depth as a function of scale factor:

$$\tau(a) \equiv \int_a^{a_0} \frac{da'}{a'^2}\, a' n_e(a') \sigma_T \tag{3.1}$$

We define the scale factor at photon decoupling $a_{\gamma d}$ such that $\tau(a_{\gamma d}) \equiv 1$. In this definition, we do not include the effects of cosmic reionization when calculating $n_e(a)$ for use in eq. (3.1) [11]. We apply $a_{\gamma d}$ and the input cosmology to equations (2.4) and (2.11) to compute the sound horizon and photon diffusion length, respectively. We arrive in this way at a ratio $(r_s/r_d)^{\rm (inp)}$ for our input cosmology.

Our immediate objective is to determine a value of $N_{\rm eff}$ (here termed $\tilde{N}_{\rm eff}$) corresponding to this value for $(r_s/r_d)^{\rm (inp)}$. We map out a range of values of r_s/r_d that correspond to the same input cosmology as that used in calculating $(r_s/r_d)^{\rm (inp)}$, with one significant difference. We parametrize all of the neutrino and BSM physics into the single $N_{\rm eff}^{\rm (th)}$ parameter. We then use $N_{\rm eff}^{\rm (th)}$ to calculate the radiation energy density in eq. (2.12) to determine the Hubble rate. We vary $N_{\rm eff}^{\rm (th)}$ to compute the function

$$r_s/r_d = r_s/r_d \left[\omega_b, \omega_c, Y_P, \ldots; N_{\rm eff}^{\rm (th)} \right], \tag{3.2}$$

shown in figure 2. Since r_s/r_d is a one-to-one function of $N_{\rm eff}^{\rm (th)}$, we may invert eq. (3.2) to obtain $N_{\rm eff}^{\rm (th)} = N_{\rm eff}^{\rm (th)}[r_s/r_d]$. The final step is to evaluate the previous function with our input cosmology ratio, i.e. $\tilde{N}_{\rm eff} = N_{\rm eff}^{\rm (th)}[r_s/r_d = (r_s/r_d)^{\rm (inp)}]$, to obtain a value of $\tilde{N}_{\rm eff}$. As an example, we take the best-fit values from ref. [11] combined with WMAP Polarization data ($100\theta_s = 1.04136$ & $100\theta_d = 0.161375$) to obtain $(r_s/r_d)^{\rm (inp)} = 100\theta_s/100\theta_d = 6.45304$. This corresponds to a value $\tilde{N}_{\rm eff} = 3.31$ on figure 2, in line with the best-fit value $N_{\rm eff} = 3.25$ ($3.51^{+0.80}_{-0.74}$ at 95% limits) [11]. We again note that for the simplest cosmologies the two generally distinct functions $N_{\rm eff}^{\rm (th)}[r_s/r_d]$ and $\tilde{N}_{\rm eff}[r_s/r_d]$ reduce to the same function and have $N_{\rm eff}^{\rm (th)} = \tilde{N}_{\rm eff}$.

Figure 2, which shows the function $r_s/r_d[N_{\rm eff}^{\rm (th)}]$, demonstrates an important constraint between phenomena occurring during the epochs of BBN and recombination/photon decoupling. For a given input cosmology ($\omega_b, \omega_c, \ldots$), the graph of r_s/r_d as a function of $N_{\rm eff}^{\rm (th)}$ requires a computation of $n_e(a)$ to obtain r_d for each value of $N_{\rm eff}^{\rm (th)}$.

We can understand figure 2 qualitatively by a simple scaling argument. We expect that, as the radiation energy density increases with increasing $N_{\rm eff}^{\rm (th)}$, the sound horizon and the diffusion length will decrease with the increasing Hubble rate $H(a)$. The sound horizon decreases due to the increased energy density driving a more rapid expansion and a decrease in the sound speed, $c_s = [3(1 + R(a))]^{-1/2}$. The diffusion length increases, naively, due to a decrease in the scattering rate driven by the reduced Hubble time. Caution should be taken when using such naive scaling arguments. For example, the non-trivial dependence of the recombination history leads to counterintuitive effects in the $\tilde{N}_{\rm eff}$ dependence on $\sum m_\nu$ [42].
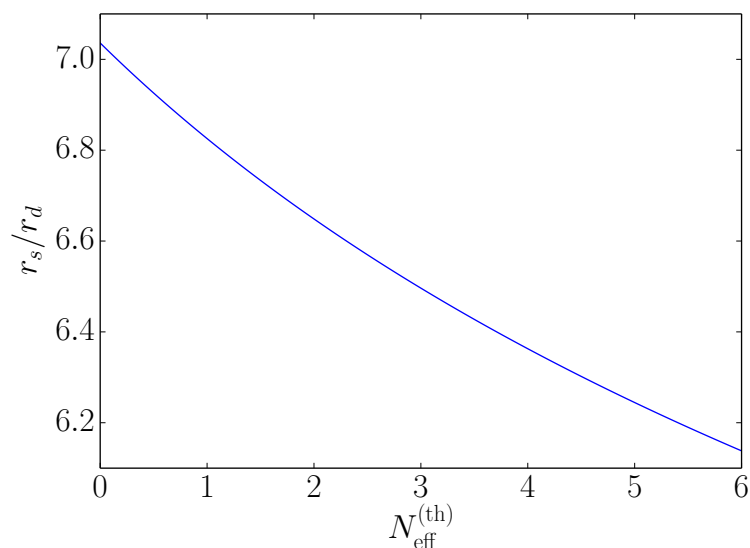
Figure 2. Ratio of the comoving coordinate of the sound horizon radius r_s to that of the photon diffusion length r_d as a function of $N_{\text{eff}}^{(\text{th})}$ for cosmological parameter values $Y_P = 0.2425$, $\omega_b = 0.22068$, and $\omega_c = 0.12029$.

Ref. [42] demonstrates that where a naive scaling argument would suggest an increase in $\tilde{N}_{\text{eff}}$ with increasing $\sum m_\nu$, the non-trivial dependence of the recombination history on $\sum m_\nu$ implies $\tilde{N}_{\text{eff}}$ decreases monotonically and rapidly with increasing $\sum m_\nu$ (See section 5.1).

4 Verification of cosmological parameters with dark radiation

We adopt the point of view advocated in refs. [10, 27, 28] that the constraint provided by predictions of BBN should be incorporated simultaneously with constraints due to recombination effects in the extraction of cosmological parameters. We also require, as previously discussed, that BBN and recombination be solved iteratively. In this section, we demonstrate the self-consistent extraction of these parameters by employing a simple model for the radiation energy density that avoids solving, for example, the Boltzmann equation, for the set of distribution functions of the cosmic constituents, in particular the neutrinos.

We follow the standard paradigm for the BBN epoch as originally discussed in ref. [19] and subsequently in refs. [20, 21]. To that extent, we use BURST to verify our results with those of other theoretical groups [43–45]. For example, at $\omega_b = 0.022068$ and $\tilde{N}_{\text{eff}} = 3.046$, ref. [11] finds:

$$Y_P = 0.24725 \pm 0.00032 \tag{4.1}$$

$$\text{D/H} = (2.656 \pm 0.067) \times 10^{-5} \tag{4.2}$$

using the code PArthENoPE [46]. This compares favorably to our values:

$$Y_P = 0.24306 \tag{4.3}$$

$$\text{D/H} = 2.631 \times 10^{-5} \tag{4.4}$$

ref. [11] includes effects of non-thermal neutrino spectral distortions [46], whereas our model only includes dark radiation. The non-thermal spectra alters the neutron to proton ratio which is the source of the disagreement for Y_P. We give a detailed description of the dark-radiation model to distinguish between it and the models of section 5.

The model we explore in this section is identical to ΛCDM except for one additional constituent: dark radiation. The dark radiation energy density is radiation at all epochs and does not interact with the other energy-density constituents through any force except gravitation.

The total energy density as given in terms of radiation, matter, and vacuum energy components is

$$\rho(a) = \rho_r(a) + \rho_m(a) + \rho_v(a), \tag{4.5}$$

which depend on the scale factor a as a^{-4}, a^{-3}, a^0, respectively, as long as there is no energy transfer between the species. We assume for the purposes of this section that the neutrinos are massless, always acting as radiation energy density. The matter energy density consists of contributions from baryons and cold dark matter. Modeling the matter as a pressureless gas and observing that the comoving matter energy density is conserved, we write the proper energy density as

$$\rho_m = \frac{3H_0^2 \, m_{\rm pl}^2}{8\pi}(\Omega_b + \Omega_c)\left(\frac{a_0}{a}\right)^3. \tag{4.6}$$

The vacuum energy is the least understood of the energy densities. Assuming the universe to be critically closed, the sum of the three energy densities must be equal to the critical energy density, specified only by the Hubble rate at the current epoch. Hence, $\rho_v = \rho_c - \rho_{r,0} - \rho_{m,0}$. The vacuum energy density is negligible at all epochs of interest in this paper but is included for completeness.

The radiation component is given as:

$$\rho_r = \rho_\gamma + \rho_\nu + \rho_{\rm dr} \tag{4.7}$$

where ρ_γ is the photon energy density, ρ_ν is the neutrino energy density, and $\rho_{\rm dr}$ is the dark-radiation energy density. We parametrize $\rho_{\rm dr}$ as

$$\rho_{\rm dr} = \frac{7}{4}\left(\frac{4}{11}\right)^{4/3}\frac{\pi^2}{30}T^4\,\delta_{\rm dr}, \tag{4.8}$$

where $\delta_{\rm dr}$ is the dark-radiation parameter and is always assumed to be non-negative. In principle, we could entertain negative values of $\delta_{\rm dr}$ since it is an adjustable parameter of ρ_r. Such a change requires a fundamental reworking of the ΛCDM model so that $\sum_i \Omega_i = 1$. These non-standard cosmologies obtain when considering, for example, neutrino oscillations. These models, however, are not continuously connected with our model at $\delta_{\rm dr} = 0$, for any values of the parameters, thus motivating the maintenance of $\delta_{\rm dr} > 0$.

We write $N_{\rm eff}^{\rm (th)} = 3 + \Delta N_{\rm eff}^{\rm (th)}$ and assume that the contribution to $N_{\rm eff}^{\rm (th)}$ from ρ_ν is 3. Then the contribution from $\rho_{\rm dr}$ is given as $\Delta N_{\rm eff}^{\rm (th)}$. We see then that $\Delta N_{\rm eff}^{\rm (th)} = \delta_{\rm dr}$. This is simply a restatement of the fact from the previous section, section 3, that $\tilde{N}_{\rm eff} = 3 + \Delta N_{\rm eff}^{\rm (th)} = N_{\rm eff}^{\rm (th)}$ for 'standard' cosmologies. It is, therefore, unnecessary for this simple dark-radiation model, to deduce $\tilde{N}_{\rm eff}$ from r_s/r_d since $N_{\rm eff}^{\rm (th)} = \tilde{N}_{\rm eff}$ by construction. This model of dark

radiation is the usual model applied, for example in ref. [11] and we explore, in this section, the predictions of the present BURST code to verify our results against those of prior results within the community. We will use $\tilde{N}_{\rm eff}$, for the remainder of this section, to denote the "effective number of relativistic degrees of freedom".[6]

Figures 3–6 show the results of computations in which the four parameters ω_b, Y_P, D/H, and $\tilde{N}_{\rm eff}$ are varied. We begin by varying the two model inputs: ω_b and $\tilde{N}_{\rm eff}$. The upper panel in figure 3 shows the dependence of $\tilde{N}_{\rm eff}$ on ω_b for curves of constant Y_P; the vertical band is the Planck value of $\omega_b = 0.02207 \pm 0.00033$. The figure is generated by first choosing a value for the baryon density in the range $0.004 \leq \omega_b \leq 0.029$. Each selected value of the dark radiation parameter in the range $3 \leq \tilde{N}_{\rm eff} \leq 4.5$ allows for the prediction of Y_P and D/H by parametrizing the radiation energy density as in eq. (2.12). The values so obtained are plotted as contours in the $\tilde{N}_{\rm eff}$-ω_b plane in the upper and lower panels of figure 3. The solid curve is the preferred value $Y_P = 0.2465 \pm 0.0097$ of ref. [7], which is a selection of observations of metal poor extragalactic H II regions. The contours are spaced by roughly $0.0097/3$ showing that $\tilde{N}_{\rm eff}$ is not strongly constrained by values of Y_P alone; this is a manifestation of the degeneracy of $\tilde{N}_{\rm eff}$ and Y_P. For example, at $Y_P = 0.2465 \pm 0.0035$, corresponding to the contours closest to $Y_P = 0.2465$, the range allowed $\tilde{N}_{\rm eff}$ is nearly consistent with both the standard, calculated value $N_{\rm eff} = 3.046$ and the ref. [11] derived value of $N_{\rm eff} = 3.30 \pm 0.27$.

Predictions of the primordial deuterium abundance are a much more sensitive constraint upon allowed values of $\tilde{N}_{\rm eff}$. This can be seen in the lower panel of figure 3. The solid line contour with $10^5 \times$ D/H $= 2.530 \pm 0.04$ corresponds to the recent measurement of ref. [8]. Contours in this figure are separated by the one standard deviation of ref. [8]. There are two points of interest regarding the deuterium figure. First, as noted in ref. [8], observation of the primordial component of deuterium is precise enough to begin to constrain the microscopic physics of the thermally averaged nuclear reaction rates and their cross sections. Additionally, given the precision of the current and forthcoming deuterium measurements and the strong dependence of $\tilde{N}_{\rm eff}$ on its value (at constant ω_b), we advocate using D/H as a prior, over Y_P, for future base model parameter searches as recommended by refs. [6, 8, 47].

The degeneracy between $\tilde{N}_{\rm eff}$ and Y_P is again evident in figure 4. Each plot explores the D/H vs. ω_b contour space, where the upper plot contains contours of constant Y_P and the lower plot contains contours of constant $\tilde{N}_{\rm eff}$. The shaded bands in each figure indicate the one-sigma observations of ω_b and D/H from refs. [8, 11], respectively. Deuterium is not an input parameter into our model. We compute it by choosing a baryon number and iteratively change the dark-radiation parameter, $\delta_{\rm dr}$ until matching the chosen deuterium target. The outputs from the process are $\tilde{N}_{\rm eff}$ and Y_P. Values of ω_b, D/H and $\tilde{N}_{\rm eff}$ are in satisfactory agreement with the standard cosmology at the precision of current observations.

The quantities D/H and ω_b are the tightest observationally-constrained parameters we are currently investigating. Figure 5 shows two plots in the Y_P-$N_{\rm eff}$ plane with contours of constant ω_b (upper plot), and contours of constant $10^5 \times$ D/H (lower plot). The horizontal band in each figure indicates the one-sigma observation of Y_P from ref. [7]. Like D/H, Y_P is not an input into our model. Consequently, we adopt the identical iterative method for Y_P in figure 5 as we do for D/H in figure 4. For the ω_b (upper) plot of figure 5, the solid contour line is the best-fit value of ref. [11] with nine-sigma spacing of the contours. The contours exist in a subspace of the Y_P-$N_{\rm eff}$ plane which is well within current observations, but nevertheless could span a range of radically different physics. Similarly, the bottom plot

---

[6]We refer to $N_{\rm eff}$ as the effective number of relativistic degrees of freedom although there are factors that complicate this interpretation, among them the temperature parameter, and fermionic nature of neutrinos.
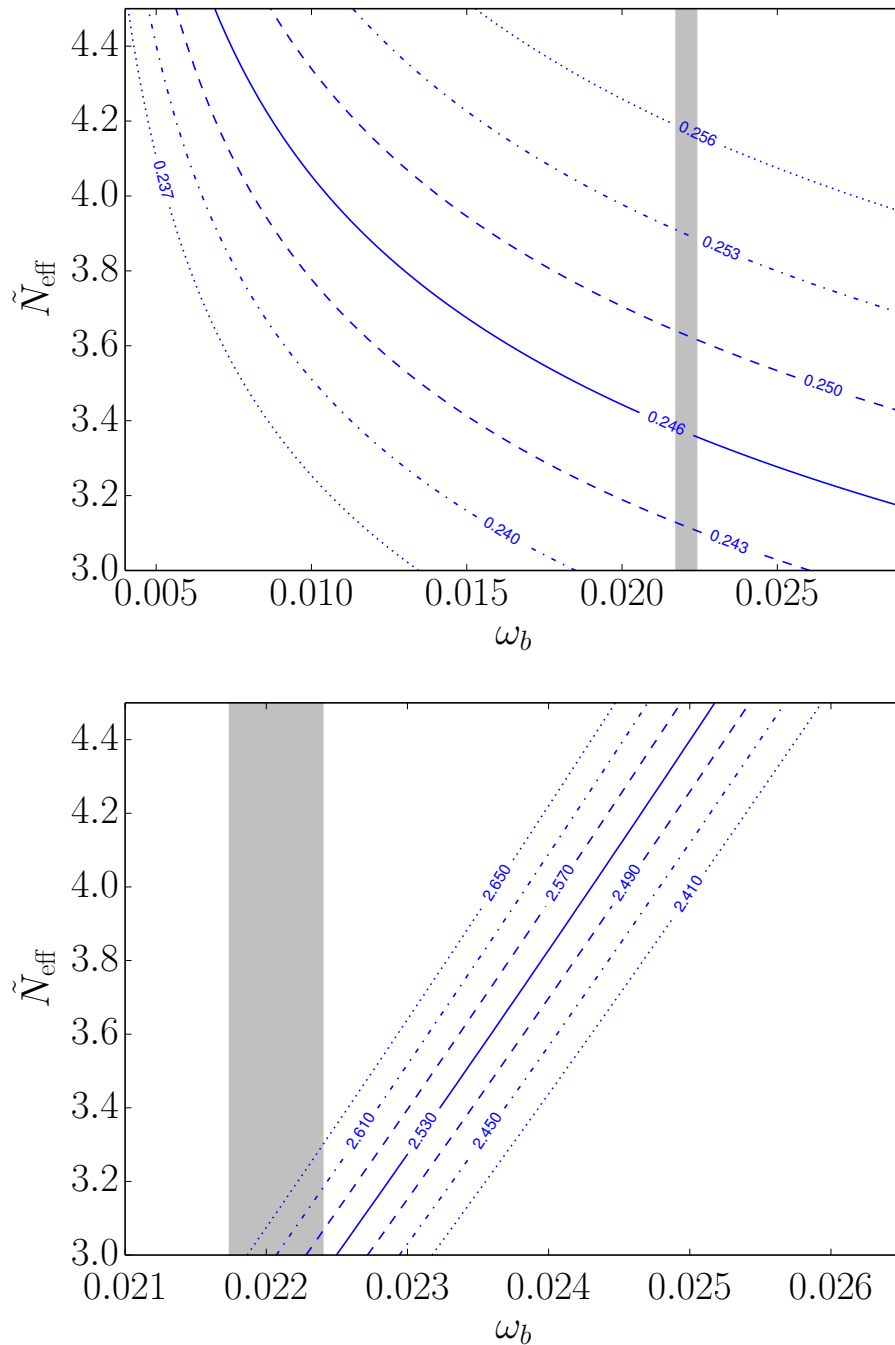
Figure 3. (Top) $\tilde{N}_{\mathrm{eff}}$ plotted against ω_b for contours of constant values of Y_P (labeled by mass fraction). The solid curve is the preferred value of ref. [7]. The contours are spaced by $\Delta Y_P \approx 0.003$. (Bottom) $\tilde{N}_{\mathrm{eff}}$ versus ω_b for contours of constant values of $10^5 \times \mathrm{D/H}$. The solid curve is the preferred value of ref. [8]. The contours are spaced by $\Delta(10^5 \times \mathrm{D/H}) = 0.04$. In each case, abundances are determined in a self-consistent BBN calculation.
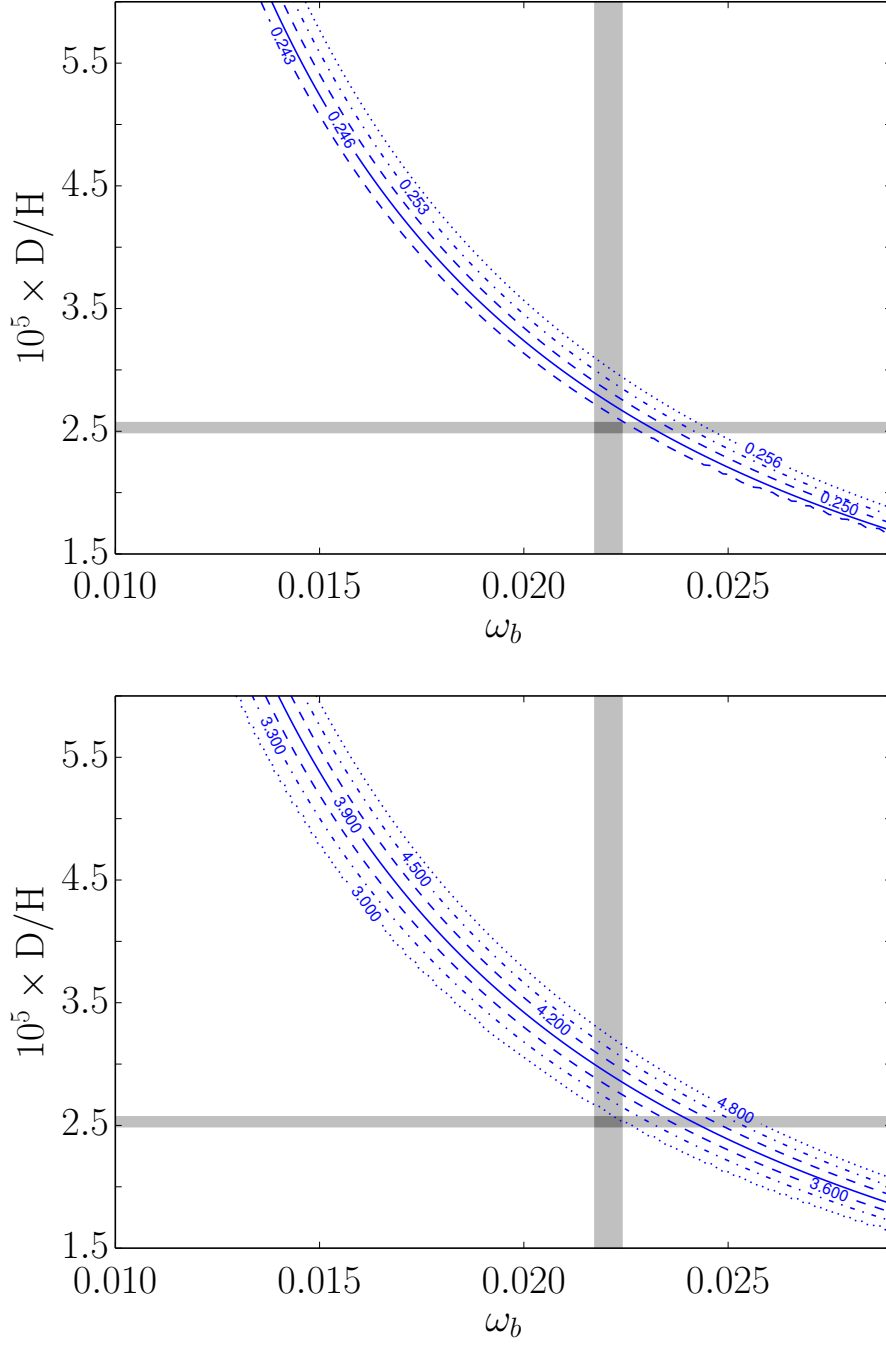
Figure 4. (Top) $10^5 \times \mathrm{D/H}$ plotted against ω_b for contours of constant Y_P. The solid curve is the preferred value of ref. [7]. The contours are spaced by $\Delta Y_P \approx 0.003$. (Bottom) $10^5 \times \mathrm{D/H}$ versus ω_b for contours of constant $\tilde{N}_{\mathrm{eff}}$. The contours are spaced by $\Delta \tilde{N}_{\mathrm{eff}} = 0.3$
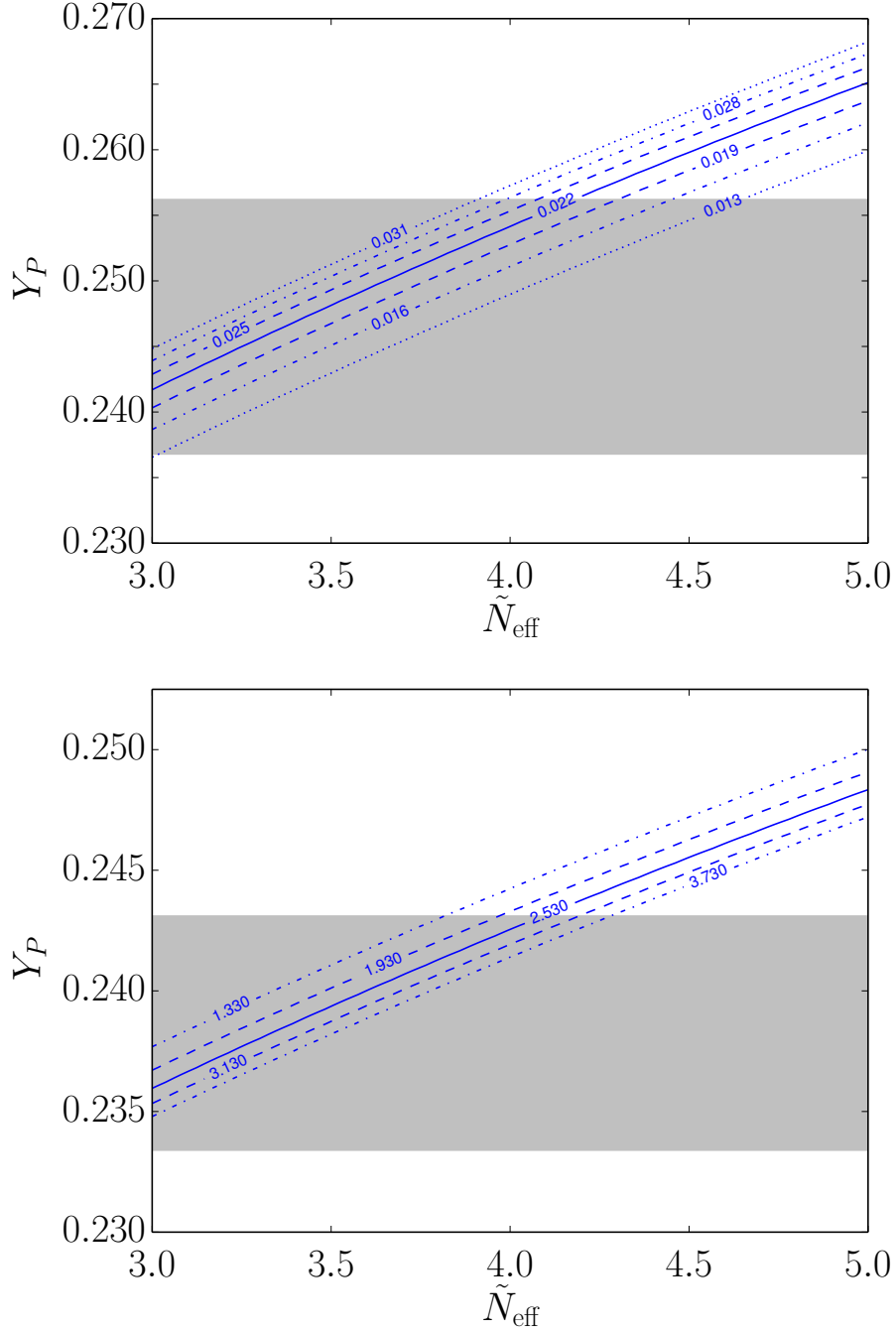
Figure 5. (Top) Y_P plotted against $\tilde{N}_{\text{eff}}$ for contours of constant ω_b. The solid curve is the best-fit value of ref. [11]. The contours are spaced by $\Delta\omega_b = 0.003$. (Bottom) Y_P versus $\tilde{N}_{\text{eff}}$ for contours of constant $10^5 \times \text{D/H}$. The solid curve is the preferred value of ref. [8]. The contours are spaced by $\Delta(10^5 \times \text{D/H}) = 0.6$.
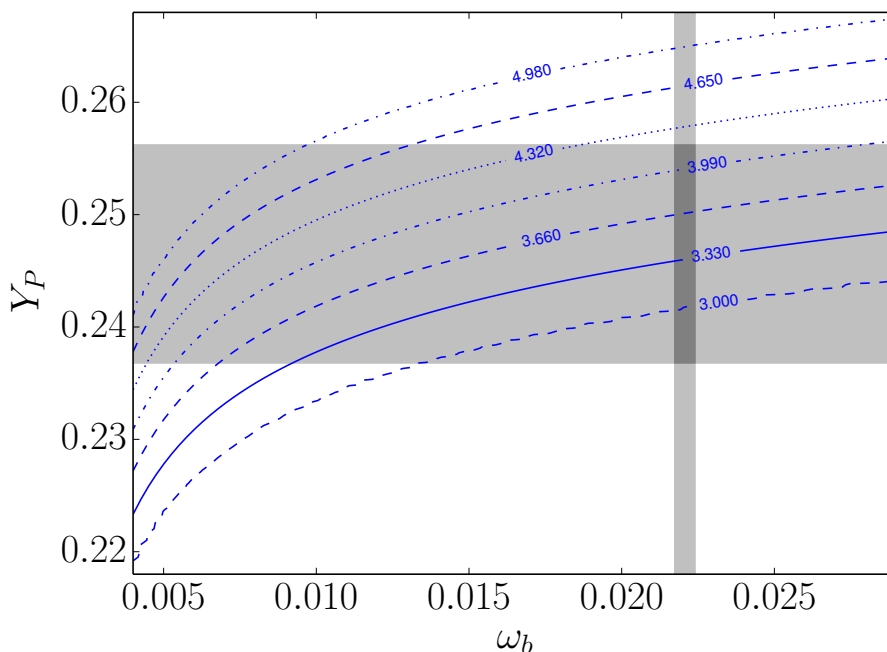
Figure 6. Y_P plotted against ω_b for contours of constant $\tilde{N}_{\mathrm{eff}}$. The contours are spaced by $\Delta \tilde{N}_{\mathrm{eff}} = 0.33$.

shows the $10^5 \times$ D/H value of ref. [8] as the solid contour with the other contours spaced fifteen-sigma apart. Clearly, Y_P and $\tilde{N}_{\mathrm{eff}}$ do not constrain the cosmological model as tightly as ω_b and D/H. This observation indicates the import of using the next generation of 30-meter class telescopes and CMB observation to better determine the light element abundances, particularly, Y_P with high precision.

Figure 6 shows how $\tilde{N}_{\mathrm{eff}}$ changes in the Y_P-ω_b plane. The shaded bands in each figure indicate the one-sigma observations of ω_b and Y_P from refs. [7, 11], respectively. We may conclude from this plot that there could exist many different values of $\tilde{N}_{\mathrm{eff}}$ consistent with the observations of Y_P and ω_b. However, we caution against such a conclusion without considering the effect on D/H. In fact, we choose not to include a figure of contours of D/H in the Y_P-ω_b plane because the strong sensitivity of D/H to ω_b produces too large a range of values for Y_P to be useful as a constraint of the cosmological model.

All calculations show a consistency between ω_b, $\tilde{N}_{\mathrm{eff}}$, D/H, and Y_P to a conservative limit of two-sigma error range in each observation. We expect the uncertainties in each observation to improve in the coming years with large ground-based CMB experiments [48, 49] and 30-meter class telescopes [50–52]. Future high-precision measurements may result in tensions for the best-fit values of ω_b, $\tilde{N}_{\mathrm{eff}}$, and D/H. These tensions could be indications of the need for more precise theoretical and numerical approaches or could signal the presence of physics beyond the standard model. As it stands here, the bottom panels of figures 3 and 4 shows that the tension between ω_b and D/H cannot be resolved with the addition of extra radiation energy density. Uncertainties in nuclear reactions may produce disagreement between ω_b and D/H, allowing D/H to become a probe of nuclear physics. It is also possible that the spectroscopic determination of D/H may be subject to small systematic errors only recognizable at such precision. An exciting prospect is the need to revise the CSM to resolve
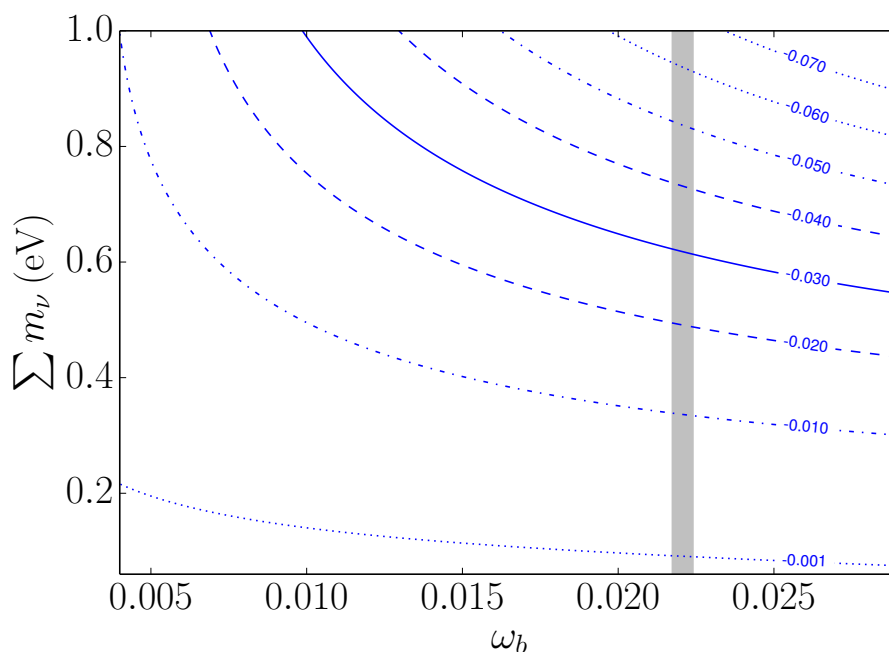
Figure 7. Determination of $\sum m_\nu$ plotted against ω_b at constant $\Delta\tilde{N}_{\text{eff}}$. The contours are spaced by ≈ 0.01 in values of $\Delta\tilde{N}_{\text{eff}}$. All contours correspond to $\Delta\tilde{N}_{\text{eff}} < 0$.

tensions with the observations of D/H and ω_b, possibly leading to the conclusion of BSM physics active during BBN.

5 Examples for neutrino sector BSM physics

We describe three examples of unresolved issues in BSM/CSM physics, which require the fully self-consistent parameter determination described in previous sections. We consider, in turn, models incorporating neutrino rest mass, sterile neutrinos, and non-zero lepton numbers. We use, throughout this section, the observationally-inferred definition of N_{eff}, $\tilde{N}_{\text{eff}}$.

5.1 Neutrino rest mass

Section 4 details a self-consistent treatment of the BBN observables Y_P, D/H, $\tilde{N}_{\text{eff}}$, and ω_b. The sum of the light neutrino masses, denoted $\sum m_\nu$, has no bearing on the determination of primordial abundances in BBN calculations due to the high temperatures relevant there. Here, however, we explore the epochs and energy scales in the history of the universe associated with the $\sum m_\nu$ energy scale in order to investigate the relationship between $\sum m_\nu$ and the other four observables of interest (ω_b, $\tilde{N}_{\text{eff}}$, Y_P and D/H). Specific examples of such epochs that we might consider include the surface of last scattering ($z \sim 1100$) and the advent of LSS ($z \lesssim 10$). We focus on the surface of last scattering and implications for the CMB in this paper.

Reference [42] (hereafter GFKPI) investigates the effect of neutrino rest mass on $\tilde{N}_{\text{eff}}$ using the BURST suite of codes. Conventional estimates based on the energy density added by non-zero neutrino rest masses suggest an increase in $N_{\text{eff}}^{(\text{th})}$. However, using the method

– 17 –

outlined in section 3, GFKPI shows a decrease in $\tilde{N}_{\text{eff}}$. The decrease is due to an effect on the recombination history stemming from an increase in the Hubble rate, which results in a larger free-electron fraction. This counterintuitive result is termed the "neutrino-mass/recombination (νMR) effect". The νMR effect manifests itself only in a self-consistent treatment, such as that employed by GFKPI.

In addition, GFKPI investigates the dependence of the νMR effect on ω_b. We revisit this physics here in preparation for a discussion on the effect of non-zero lepton number L_ν later, in section 5.3.2. Increasing ω_b leads to an enhancement of the νMR effect when $\sum m_\nu$ is held constant, as is evident by the curvature of the contours in figure 7. The enhancement is a consequence of the effect that changing ω_b has on the the recombination history. We might naively expect a larger change in the Hubble rate relative to the massless neutrino case resulting in an enhanced νMR effect for the smaller ω_b case. This is opposite to that observed in figure 7. This result also is counterintuitive based on expectations from a simple scaling of the energy density and the resulting change in the recombination history [42].

The origin of the enhancement of the νMR effect can be understood by considering a simplification of the Boltzmann equation that determines the recombination history [eq. (2.10)]. We take $Y_P = 0$ for the purposes of this argument since the νMR enhancement is insensitive to Y_P, as we have verified numerically for the ranges of parameters we are considering. In this simple scenario, $X_e = X_p$ and we obtain an expression for the change in the free-electron fraction:

$$\frac{dX_e}{dt} = (1 - X_e)\beta - X_e^2 n_e^{(\text{tot})}\alpha^{(2)}, \tag{5.1}$$

where $\beta \equiv \alpha^{(2)}(m_e T/2\pi)^{3/2}e^{-\Delta Q/T}$ is the ionization coefficient and $\alpha^{(2)}$ is the recombination coefficient with $\Delta Q = 13.6\,\text{eV}$.

Equation (5.1) for the recombination history shows that the free-electron disappearance rate is proportional to the total electron number density, which in turn is proportional to ω_b through eq. (2.9). Equation (2.9) also shows how $n_e^{(\text{tot})}$ relates to Y_P. Note that ω_b and Y_P affect $n_e^{(\text{tot})}$ differently. However, due to the relative insensitivity of Y_P to ω_b, the ω_b dependence dominates in eq. (2.9). The increase in energy density from $\sum m_\nu \neq 0$ and the increase in the free-electron disappearance rate combine to alter the recombination history so as to enhance the νMR effect for increasing ω_b.

5.2 Sterile neutrinos

We next consider the possibility that there exists either single or multiple sterile-neutrino species, which could have profound implications in cosmology. We entertain two possibilities of either light or heavy sterile neutrinos.

5.2.1 Light sterile neutrinos

Observations of neutrino events in large scintillating detectors may have revealed anomalies that could be interpreted as sterile neutrinos with rest masses $m_{\nu_s} \sim 1\,\text{eV}$ [53–55]. We investigate the presence of a single sterile neutrino in the early universe by employing a model where the sterile state populates a thermal Fermi-Dirac shaped distribution with temperature parameter T_s, possibly through flavor mixing. The sterile neutrino temperature, T_s is taken to be less than or equal to the active neutrino temperature T_ν. The ratio T_s/T_ν is assumed to be the same throughout weak decoupling, BBN, and recombination. For this analysis, we do not investigate smaller active-sterile neutrino mixing angles with resultant non Fermi-Dirac-shaped energy spectra [41, 56]. Future work will consider such physics [57].
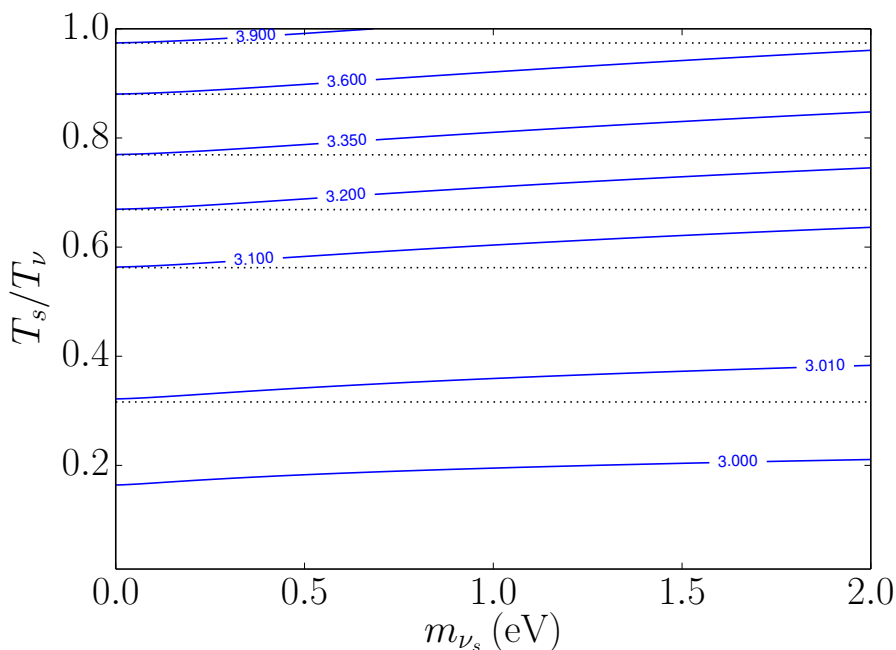
Figure 8. Ratio of the sterile to active neutrino temperatures, T_s/T_ν, plotted against m_{ν_s} for contours of constant $\tilde{N}_{\text{eff}}$ for $\sum m_\nu = 0.06\,\text{eV}$. Horizontal dotted lines show the prediction if the sterile neutrino was massless, i.e. $m_{\nu_s} = 0$.

Figure 8 displays contours of constant $\tilde{N}_{\text{eff}}$. The vertical axis is the ratio T_s/T_ν and the horizontal axis the sterile neutrino rest mass m_{ν_s}. We maintain the ratio $T_\nu/T = (4/11)^{1/3}$, assuming covariant conservation of entropy, starting at the end of the epoch of $e^\pm$-annihilation and continuing throughout the remainder of the history of the universe. The dotted lines show the expectation from the dark radiation analysis of section 4 without employing the self-consistent, iterative approach developed in section 3. The deviation of the contours from the dotted lines is again due to an effect similar to the νMR effect but, in this instance, due to the sterile state. Figure 8 takes the sum of the active neutrino masses to be 0.06 eV. This is inconsequential for large $T_s/T_\nu \lesssim 1$. For $T_s/T_\nu \lesssim 0.1$, $\Delta\tilde{N}_{\text{eff}} < 0$ due to the νMR effect in the active neutrino sector. As a consequence, the contour for $\tilde{N}_{\text{eff}} = 3$ is not coincident with the m_{ν_s} axis. Since m_{ν_s} is too small to be of any significant kinematic effect during BBN, we need only compute BBN once for a given value of T_s/T_ν. During recombination, m_{ν_s} is kinematically important and affects the Hubble rate. Hence, for every point in the T_s/T_ν-m_{ν_s} plane of figure 8 we calculate recombination. This figure clearly emphasizes the need for a self-consistent treatment between BBN and recombination when considering this BSM physics.

5.2.2 Heavy sterile neutrinos

Heavy sterile neutrinos that decay out of equilibrium in the early universe can affect weak decoupling and, as a consequence, primordial nucleosynthesis [16, 58, 59]. Sterile neutrinos in the rest mass range $0.1\,\text{GeV} \leq m_{\nu_s} \leq 1.0\,\text{GeV}$, with lifetimes $\gtrsim 1$ s decaying during the weak decoupling, weak freeze-out, and/or BBN epochs can have constrainable, sometimes dramatic, cosmological effects.

Such sterile neutrinos have mass and vacuum mixings with ν_e, ν_μ, ν_τ constrained by accelerator and other laboratory oscillation experiments/observations [60–67], beta-decay experiments [68], and cosmological considerations, including constraints on $\sum m_\nu$ and N_{eff} [69–76]. In fact, stringent constraints can be obtained from N_{eff} limits alone [16], as sterile neutrinos decaying out of equilibrium can lead to dilution (entropy production) which, in the weak decoupling epoch, can lead to distortions in the relic neutrino energy spectrum, affecting $\sum m_\nu$, and have significant impact on the relativistic energy content and, hence, N_{eff}. A sophisticated theoretical and computational treatment of dilution physics is a challenging endeavor. We have developed BURST to address this specific problem. BURST employs individual neutrino spectra for each species, binned according to the co-moving quantity $\epsilon \equiv E/T_\nu$. The binned-spectra evolve with the universe as heavy particles decay, injecting entropy into the neutrino seas, and subsequently equilibrate by scattering on background neutrinos and electrons and positrons. We track multiple decades of ϵ values over many Hubble times. Our Boltzmann solver calculates the rates for each individual scattering process so we can decipher the contributions of each process to the shape of the neutrino spectra. Even though these heavy sterile neutrinos may decay away before an epoch where $T \sim 10$ keV, they can nevertheless alter the relationship between Y_P, D/H, N_{eff}, $\sum m_\nu$, and ω_b, necessitating the need for a self-consistent treatment between the weak decoupling, weak freeze-out, BBN, recombination, photon decoupling, and advent of LSS epochs [77].

5.3 Lepton numbers

We examine how lepton numbers affect the primordial abundances and $\tilde{N}_{\text{eff}}$. We define the lepton number L_ν for a neutrino species ν in a flavor eigenstate as

$$L_\nu \equiv \frac{n_\nu - n_{\bar\nu}}{n_\gamma}, \tag{5.2}$$

where n_ν is the number density of neutrino species ν, $n_{\bar\nu}$ is the number density of antineutrino species $\bar\nu$, and n_γ is the number density of photons. Here, for illustrative purposes, we take $L_{\nu_e} = L_{\nu_\mu} = L_{\nu_\tau} \equiv L_\nu$.

The efficiency of neutrino oscillations in equating lepton numbers is approximate, and indeed dependent on neutrino physics [78–80]. In fact, ref. [79] shows that oscillations with solar mass-splitting scales cause disparate lepton numbers in e, μ, τ neutrinos to equilibrate to within an order of magnitude of one another. The limitations of existing calculations revolve around how quantum damping and neutrino energy dependence are handled.

We use the comoving-invariant neutrino degeneracy parameter $\xi_\nu \equiv \mu_\nu/T_\nu$, where μ_ν is the chemical potential of neutrino ν, to compute L_ν. The present model assumes that the lepton number evolves through the epoch of $e^\pm$ annihilation only in response to the relative increase in n_γ. We do not consider any BSM physics which could alter the difference $n_\nu - n_{\bar\nu}$; that is, we fix ξ_ν throughout weak decoupling, BBN, and photon decoupling. We relate the degeneracy parameter to the lepton number using the following expression [56, 81, 82]:

$$L_\nu = \frac{4}{11} \frac{1}{12\zeta(3)} \left(\pi^2 \xi_\nu + \xi_\nu^3 \right), \tag{5.3}$$

where $\zeta(3) \approx 1.202$. The factor 4/11 in eq.(5.3) implies that our lepton numbers refer to the post $e^\pm$ annihilation epoch, where $T_\nu/T = (4/11)^{1/3}$.
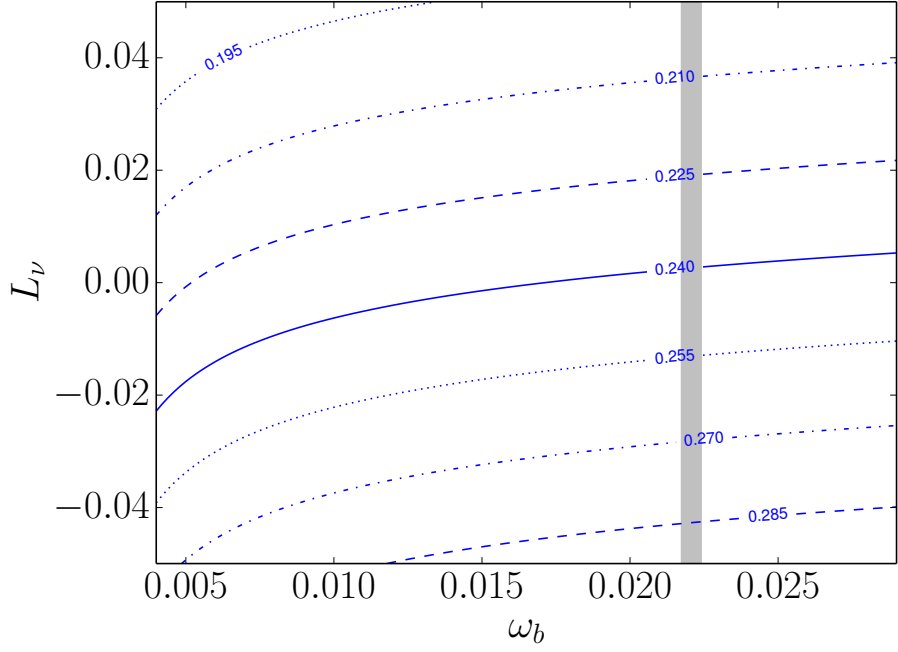
Figure 9. Lepton asymmetry L_ν [eq.(5.2)] plotted against ω_b for contours of constant Y_P. The contours are spaced by $\Delta Y_P = 0.015$.
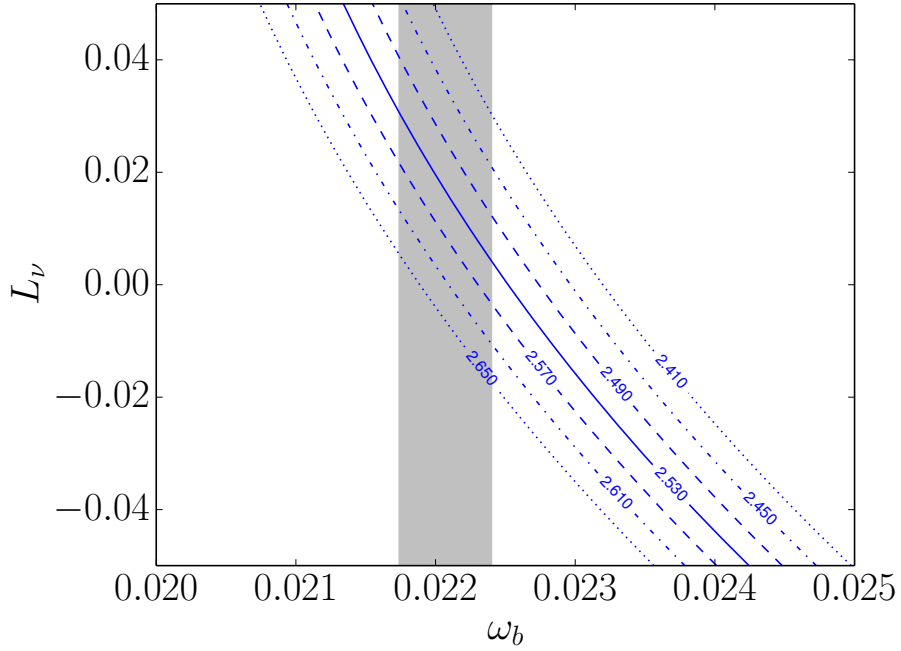

Figure 10. Lepton asymmetry L_ν plotted against ω_b for contours of constant $10^5 \times \mathrm{D/H}$. The solid curve is the preferred value of ref. [8]. The contours are spaced by $\Delta(10^5 \times \mathrm{D/H}) = 0.04$.

5.3.1 Effect on nucleosynthesis

The helium mass fraction is sensitive to the neutron-to-proton ratio, n/p. We determine n/p by calculating the weak rates associated with neutrino-nucleon reactions, namely:

$$\nu_e + n \rightleftharpoons e^- + p^+ \tag{5.4}$$

$$\bar{\nu}_e + p^+ \rightleftharpoons e^+ + n \tag{5.5}$$

and in addition, neutron and inverse neutron decay:

$$n \rightleftharpoons e^- + \bar{\nu}_e + p^+ \tag{5.6}$$

The net rates in reactions (5.4) and (5.5) fall below the Hubble rate at the epoch of weak freeze-out. Weak freeze-out largely precedes the alpha-particle formation process in BBN, though unlike the brief time/temperature range of α-formation, weak freeze-out occurs over several Hubble times at this epoch. The rates in reactions (5.4) through (5.6) are sensitive to the neutrino and $e^\pm$ distributions. We follow ref. [21] to evolve T and the electron chemical potential in order to maintain equilibrium between the electrons, positrons and photons. For the electron-flavor neutrinos, we use the comoving invariants aT_ν and ξ_{ν_e} to compute the neutrino distributions. We set $\sum m_\nu = 0$ as neutrinos of sub-eV rest mass remain ultra-relativistic throughout weak freeze-out.

Figures 9 and 10 show the helium mass fraction and the relative deuterium abundance, respectively. Each plot is in the L_ν-ω_b plane for contours of constant primordial abundance. The relationships between lepton number and nucleosynthesis are well known [47, 83]. Increasing L_{ν_e} leads to an overabundance of neutrinos compared to anti-neutrinos. The forward rate of reaction (5.4) freezes-out after the forward rate of reaction (5.5). The imbalance lowers n/p which lowers Y_P as seen in figure 9. The decrease in n/p also leads to a decrease in D/H, although deuterium is not as sensitive to L_ν as helium. However, D/H is known to much higher precision than is Y_P.

Comparing with recent observations [7, 8], the two light element abundances achieve consistency at 2σ. Y_P prefers a value of $L_\nu < 0$ whereas D/H prefers a positive value of L_ν. If future observations of the light-element abundances were to show a larger disagreement than 2σ, lepton numbers of identical value could not solely rectify the tension. Future analyses will consider scenarios with multiple facets of BSM physics including non-zero lepton numbers [84]. This analysis will use $\tilde{N}_{\text{eff}}$ as a discriminating factor.

5.3.2 Effect on N_{eff}

We consider how two aspects of non-CSM/BSM physics ($L_\nu \neq 0$ and/or $\sum m_\nu \neq 0$) modify $\tilde{N}_{\text{eff}}$. If we set the neutrino rest mass to $\sum m_\nu \neq 0$, we can investigate whether the νMR effect still applies with non-zero L_ν. Figure 11 shows the changes to $\tilde{N}_{\text{eff}}$ in the $\sum m_\nu$-ω_b plane for three values of $L_\nu = -0.05, 0, 0.05$ corresponding to blue, magenta, and red contours, respectively. The non-zero lepton number increases $\tilde{N}_{\text{eff}}$ for small values of $\sum m_\nu$ in accordance with ref. [9]. However, for values of $\sum m_\nu \sim 1.0\,\text{eV}$, the νMR effect overwhelms the extra energy density from more particles to lower $\tilde{N}_{\text{eff}}$ below three.

Figure 11 also shows that, despite the total energy density being insensitive to the sign of L_ν, the contours for non-zero values of L_ν with opposite sign do not overlap because Y_P depends sensitively on its value. Y_P is largest for the blue contours, so more helium suppresses the νMR effect.
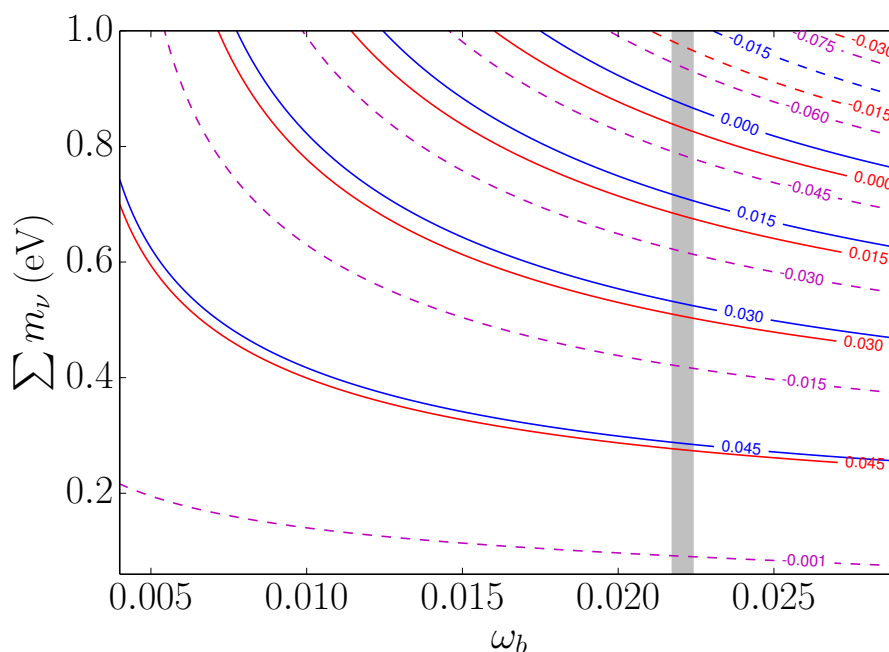
Figure 11. $\sum m_\nu$ plotted against ω_b for contours of constant $\Delta \tilde{N}_{\text{eff}}$. The blue contours are for $L_\nu = -0.05$. The magenta contours are for $L_\nu = 0$. The red contours are for $L_\nu = 0.05$. Solid contours are for positive values; dashed contours are for negative values.

Note that taking $L_\nu \neq 0$ conflates the interpretation that the effect of $\sum m_\nu$ is identical to perturbations in the matter power spectrum, which are used in calculating the suppression of power on small scales. This is borne out by the present model where the $\sum m_\nu$ statistic cannot be equated to the cosmological measurement. In our model, $\sum m_\nu$ is simply the sum of the active vacuum neutrino mass eigenvalues. The observationally determined value of $\sum m_\nu$ depends on quantities other than the sum of the active neutrino masses such as their energy distributions.

6   Conclusions and outlook

Cosmological considerations are a key route to exploring BSM physics. This is especially true for the neutrino sector, where there are many outstanding questions and where laboratory experiments are limited in what aspects of this physics can be addressed. In this paper we have argued that a self consistent treatment of BSM issues, across all epochs from weak decoupling to photon decoupling, is the best way to take advantage of the expected coming increase in precision of CMB measurements and observationally-inferred primordial abundances of the light elements. We employ a limited prescription to link the salient features of self consistency between early-time neutrino dynamics and the surface of last scattering. We couple the weak decoupling and nucleosynthesis of early times to CMB observables, including baryon-to-photon ratio (equivalently ω_b), sound horizon, and photon diffusion length.

We have shown that such a self consistent treatment is necessary, in part because new neutrino physics can alter the relationships between different cosmological epochs. For example, ω_b and other CMB observables affect the calculated yields of deuterium and helium.

In addition, the calculated relic neutrino energy spectra after weak decoupling affects the predicted value of $\tilde{N}_{\rm eff}$ at photon decoupling. The principal tool in our analysis is the suite of BURST codes for nucleosynthesis and neutrino interactions and energy transport.

A case in point is our investigation of the relationship between neutrino rest masses, i.e. $\sum m_\nu$, and the four potential observables ω_b, $\tilde{N}_{\rm eff}$, Y_P, and D/H. This analysis reveals the "neutrino-mass/recombination" (νMR) effect first described in ref. [42]. The νMR effect is below the threshold of current CMB capabilities, but may not be in future observations [85].

There have been spectacular advances in the measurements/observations of neutrino properties. We know the neutrino mass-squared differences and three of the four parameters in the unitary transformation between the energy eigenstates (mass states) and the weak interaction eigenstates (flavor states) of the three active neutrinos (only the CP-violating phase remains unmeasured). As active neutrinos mix in vacuum and have non-zero rest masses, the question indubitably arises of whether there exist "sterile" neutrino states. If indeed sterile neutrinos do exist, we acknowledge that the parameter space of mass, vacuum mixing angle, and number is enormous. However, sterile neutrinos could have profound effects in all of the epochs under study in this paper. This possibility makes a self consistent treatment of these effects a powerful basis for constraining sterile neutrino states.

In this paper we have considered scenarios for both "light" (mass $\sim 1\,{\rm eV}$) and "heavy" (mass ~ 0.1–$1\,{\rm GeV}$) sterile neutrinos. In the former case we consider cases where the sterile neutrino relic energy spectra are Fermi-Dirac black-body shaped, though with a temperature parameter T_s differing from that characterizing the relic energy spectra of active neutrino species. We show here that the νMR effect has interesting consequences and that this case *demands* a self consistent treatment of recombination and BBN. Additionally, heavy sterile neutrino decay out of equilibrium can lead to dilution and high energy relic active neutrinos, and both of these features potentially can have dramatic and constrainable effects on CMB-epoch observables. This implies that CMB observations can indirectly probe the CνB and explore active-sterile mass/vacuum-mixing parameter space unavailable to current accelerator-based experiments.

We have also studied the effects of non-zero lepton numbers on the relationship between CMB observables, nucleosynthesis, and neutrino physics. Our conclusion is that the primordial deuterium abundance is a potentially powerful probe of lepton number. However, an eventual CMB-*only* measurement of the primordial helium abundance Y_P will be the most powerful probe of lepton number and many other issues. Determining Y_P from CMB observables will require a sophisticated self-consistent approach to BBN, neutrino physics, and photon decoupling transport physics.

Finally, our study has revealed a potential tension between $\tilde{N}_{\rm eff}$, ω_b, and the primordial deuterium abundance, D/H, inferred from high redshift QSO absorption systems. In fact, if the advent of 30-m class telescopes in the near future allows for a decrease in errors in observationally-inferred D/H to the $\sim 1\,\%$ level, while observed ω_b and $\tilde{N}_{\rm eff}$ maintain their respective current central values, then tension is unavoidable. This may signal BSM or non-CSM physics, likely in the neutrino sector, or it could point to not understanding systematics in the damped Lyman-α cloud measurements of the isotope-shifted hydrogen absorption lines. We advocate using future instruments to explore the rich physics of weak decoupling, nucleosynthesis, and photon decoupling to discover what role BSM neutrino physics has in these epochs.

Acknowledgments

References

[1] WMAP collaboration, G. Hinshaw et al., *Nine-Year Wilkinson Microwave Anisotropy Probe (WMAP) Observations: Cosmological Parameter Results*, *Astrophys. J. Suppl.* **208** (2013) 19 [arXiv:1212.5226] [INSPIRE].

[2] ATACAMA COSMOLOGY TELESCOPE collaboration, J.L. Sievers et al., *The Atacama Cosmology Telescope: Cosmological parameters from three seasons of data*, *JCAP* **10** (2013) 060 [arXiv:1301.0824] [INSPIRE].

[3] R. Keisler, C.L. Reichardt, K.A. Aird, B.A. Benson, L.E. Bleem et al., *A Measurement of the Damping Tail of the Cosmic Microwave Background Power Spectrum with the South Pole Telescope*, *Astrophys. J.* **743** (2011) 28 [arXiv:1105.3182] [INSPIRE].

[4] PLANCK collaboration, P.A.R. Ade et al., *Planck 2013 results. I. Overview of products and scientific results*, *Astron. Astrophys.* **571** (2014) A1 [arXiv:1303.5062] [INSPIRE].

[5] Y.I. Izotov and T.X. Thuan, *The primordial abundance of ^4He: evidence for non-standard big bang nucleosynthesis*, *Astrophys. J.* **710** (2010) L67 [arXiv:1001.4440] [INSPIRE].

[6] M. Pettini and R. Cooke, *A new, precise measurement of the primordial abundance of Deuterium*, *Mon. Not. Roy. Astron. Soc.* **425** (2012) 2477 [arXiv:1205.3785] [INSPIRE].

[7] E. Aver, K.A. Olive, R.L. Porter and E.D. Skillman, *The primordial helium abundance from updated emissivities*, *JCAP* **11** (2013) 017 [arXiv:1309.0047] [INSPIRE].

[8] R.J. Cooke, M. Pettini, R.A. Jorgenson, M.T. Murphy and C.C. Steidel, *Precision measures of the primordial abundance of deuterium*, *Astrophys. J.* **781** (2014) 31.

[9] M. Shimon, N.J. Miller, C.T. Kishimoto, C.J. Smith, G.M. Fuller et al., *Using Big Bang Nucleosynthesis to Extend CMB Probes of Neutrino Physics*, *JCAP* **05** (2010) 037 [arXiv:1001.5088] [INSPIRE].

[10] J. Hamann, J. Lesgourgues and G. Mangano, *Using BBN in cosmological parameter extraction from CMB: A Forecast for PLANCK*, *JCAP* **03** (2008) 004 [arXiv:0712.2826] [INSPIRE].

[11] PLANCK collaboration, P.A.R. Ade et al., *Planck 2013 results. XVI. Cosmological parameters*, *Astron. Astrophys.* **571** (2014) A16 [arXiv:1303.5076] [INSPIRE].

[12] A. Vlasenko, G.M. Fuller and V. Cirigliano, *Neutrino Quantum Kinetics*, *Phys. Rev.* **D 89** (2014) 105004 [arXiv:1309.2628] [INSPIRE].

[13] C. Volpe, D. Väänänen and C. Espinoza, *Extended evolution equations for neutrino propagation in astrophysical and cosmological environments*, *Phys. Rev.* **D 87** (2013) 113010 [arXiv:1302.2374] [INSPIRE].

[14] J. Serreau and C. Volpe, *Neutrino-antineutrino correlations in dense anisotropic media*, *Phys. Rev.* **D 90** (2014) 125040 [arXiv:1409.3591] [INSPIRE].

[15] A. Lewis, A. Challinor and A. Lasenby, *Efficient computation of CMB anisotropies in closed FRW models*, *Astrophys. J.* **538** (2000) 473 [astro-ph/9911177] [ɪɴSPIRE].

[16] G.M. Fuller, C.T. Kishimoto and A. Kusenko, *Heavy sterile neutrinos, entropy and relativistic energy production and the relic neutrino background*, arXiv:1110.6479 [ɪɴSPIRE].

[17] K.M. Nollett and G.P. Holder, *An analysis of constraints on relativistic species from primordial nucleosynthesis and the Cosmic Microwave Background*, arXiv:1112.2683 [ɪɴSPIRE].

[18] Z. Hou, R. Keisler, L. Knox, M. Millea and C. Reichardt, *How Massless Neutrinos Affect the Cosmic Microwave Background Damping Tail*, *Phys. Rev.* **D 87** (2013) 083008 [arXiv:1104.2333] [ɪɴSPIRE].

[19] R.V. Wagoner, W.A. Fowler and F. Hoyle, *On the Synthesis of elements at very high temperatures*, *Astrophys. J.* **148** (1967) 3 [ɪɴSPIRE].

[20] R.V. Wagoner, *Synthesis of the Elements Within Objects Exploding from Very High Temperatures*, Astrophys. J. Suppl. **18** (1969) 247.

[21] M.S. Smith, L.H. Kawano and R.A. Malaney, *Experimental, computational and observational analysis of primordial nucleosynthesis*, *Astrophys. J. Suppl.* **85** (1993) 219 [ɪɴSPIRE].

[22] A.D. Dolgov, S.H. Hansen and D.V. Semikoz, *Nonequilibrium corrections to the spectra of massless neutrinos in the early universe*, *Nucl. Phys.* **B 503** (1997) 426 [hep-ph/9703315] [ɪɴSPIRE].

[23] N.Y. Gnedin and O.Y. Gnedin, *Cosmological neutrino background revisited*, *Astrophys. J.* **509** (1998) 11 [astro-ph/9712199] [ɪɴSPIRE].

[24] G. Mangano, G. Miele, S. Pastor and M. Peloso, *A Precision calculation of the effective number of cosmological neutrinos*, *Phys. Lett.* **B 534** (2002) 8 [astro-ph/0111408] [ɪɴSPIRE].

[25] R.N. Boyd, C.R. Brune, G.M. Fuller and C.J. Smith, *New Nuclear Physics for Big Bang Nucleosynthesis*, *Phys. Rev.* **D 82** (2010) 105005 [arXiv:1008.0848] [ɪɴSPIRE].

[26] G.M. Fuller and C.J. Smith, *Nuclear weak interaction rates in primordial nucleosynthesis*, *Phys. Rev.* **D 82** (2010) 125017 [arXiv:1009.0277] [ɪɴSPIRE].

[27] R. Trotta and S.H. Hansen, *Observing the helium abundance with CMB*, *Phys. Rev.* **D 69** (2004) 023509 [astro-ph/0306588] [ɪɴSPIRE].

[28] K. Ichikawa, T. Sekiguchi and T. Takahashi, *Primordial Helium Abundance from CMB: a constraint from recent observations and a forecast*, *Phys. Rev.* **D 78** (2008) 043509 [arXiv:0712.4327] [ɪɴSPIRE].

[29] Y. Ali-Haïmoud and C.M. Hirata, *HyRec: A fast and highly accurate primordial hydrogen and helium recombination code*, *Phys. Rev.* **D 83** (2011) 043513 [arXiv:1011.3758] [ɪɴSPIRE].

[30] J. Chluba and R.M. Thomas, *Towards a complete treatment of the cosmological recombination problem*, *Mon. Not. Roy. Astron. Soc.* **412** (2011) 748 [arXiv:1010.3631] [ɪɴSPIRE].

[31] S. Seager, D.D. Sasselov and D. Scott, *How exactly did the universe become neutral?*, *Astrophys. J. Suppl.* **128** (2000) 407 [astro-ph/9912182] [ɪɴSPIRE].

[32] S. Seager, D.D. Sasselov and D. Scott, *A new calculation of the recombination epoch*, *Astrophys. J.* **523** (1999) L1 [astro-ph/9909275] [ɪɴSPIRE].

[33] P.J.E. Peebles, *Recombination of the Primeval Plasma*, *Astrophys. J.* **153** (1968) 1 [ɪɴSPIRE].

[34] Y.B. Zeldovich, V.G. Kurt and R.A. Syunyaev, *Recombination of Hydrogen in the Hot Model of the Universe*, *Zh. Eksp. Teor. Fiz.* **55** (1968) 278.

[35] D. Pequignot, P. Petitjean and C. Boisson, *Total and effective radiative recombination coefficients*, Astron. Astrophys. **251** (1991) 680.

[36] D.G. Hummer and P.J. Storey, *Recombination of helium-like ions — I. Photoionization cross-sections and total recombination and cooling coefficients for atomic helium*, Mon. Not. Roy. Astron. Soc. **297** (1998) 1073.

[37] J. Silk, *Cosmic black body radiation and galaxy formation*, Astrophys. J. **151** (1968) 459 [INSPIRE].

[38] M. Zaldarriaga and D.D. Harari, *Analytic approach to the polarization of the Cosmic Microwave Background in flat and open universes*, Phys. Rev. **D 52** (1995) 3276 [astro-ph/9504085] [INSPIRE].

[39] W. Hu and M.J. White, *CMB anisotropies: Total angular momentum method*, Phys. Rev. **D 56** (1997) 596 [astro-ph/9702170] [INSPIRE].

[40] S. Weinberg, *Cosmology*, Oxford University Press, Oxford U.K. (2008).

[41] G.M. Fuller and C.T. Kishimoto, *Quantum Coherence of Relic Neutrinos*, Phys. Rev. Lett. **102** (2009) 201303 [arXiv:0811.4370] [INSPIRE].

[42] E. Grohs, G.M. Fuller, C.T. Kishimoto and M.W. Paris, *Effects of neutrino rest mass on N_{eff} and ionization equilibrium freeze-out*, arXiv:1412.6875 [INSPIRE].

[43] F. Iocco, G. Mangano, G. Miele, O. Pisanti and P.D. Serpico, *Primordial Nucleosynthesis: from precision cosmology to fundamental physics*, Phys. Rept. **472** (2009) 1 [arXiv:0809.0631] [INSPIRE].

[44] G. Miele and O. Pisanti, *Primordial Nucleosynthesis: an updated comparison of observational light nuclei abundances with theoretical predictions*, Nucl. Phys. Proc. Suppl. **188** (2009) 15 [arXiv:0811.4479] [INSPIRE].

[45] G. Miele, O. Pisanti and S. Sarikas, *Primordial nucleosynthesis and neutrino physics beyond the standard model*, J. Phys. Conf. Ser. **259** (2010) 012007 [INSPIRE].

[46] O. Pisanti, A. Cirillo, S. Esposito, F. Iocco, G. Mangano et al., *PArthENoPE: Public Algorithm Evaluating the Nucleosynthesis of Primordial Elements*, Comput. Phys. Commun. **178** (2008) 956 [arXiv:0705.0290] [INSPIRE].

[47] C.J. Smith, G.M. Fuller, C.T. Kishimoto and K.N. Abazajian, *Light Element Signatures of Sterile Neutrinos and Cosmological Lepton Numbers*, Phys. Rev. **D 74** (2006) 085008 [astro-ph/0608377] [INSPIRE].

[48] SPT-3G collaboration, B.A. Benson et al., *SPT-3G: A Next-Generation Cosmic Microwave Background Polarization Experiment on the South Pole Telescope*, Proc. SPIE Int. Soc. Opt. Eng. **9153** (2014) 91531P [arXiv:1407.2973] [INSPIRE].

[49] POLARBEAR collaboration, P.A.R. Ade et al., *A Measurement of the Cosmic Microwave Background B-Mode Polarization Power Spectrum at Sub-Degree Scales with POLARBEAR*, Astrophys. J. **794** (2014) 171 [arXiv:1403.2369] [INSPIRE].

[50] D. Silva, P. Hickson, C. Steidel and M. Bolte, *TMT Detailed Science Case: 2007*, technical report (2007).

[51] P. McCarthy and R.A. Bernstein, *Giant Magellan Telescope: Status and Opportunities for Scientific Synergy*, in proceedings of the *Thirty Meter Telescope Science Forum*, Tucson, Arizona, U.S.A., July 2014, p. 61.

[52] I. Hook, *The science case for the European Extremely Large Telescope : the next step in mankind's quest for the Universe*, (2005) http://www-astro.physics.ox.ac.uk/˜imh/ELT/Book/ELT_brochure_2.pdf.

[53] LSND collaboration, C. Athanassopoulos et al., *The Liquid scintillator neutrino detector and LAMPF neutrino source*, Nucl. Instrum. Meth. **A 388** (1997) 149 [nucl-ex/9605002] [INSPIRE].

[54] MiniBooNE collaboration, A.A. Aguilar-Arevalo et al., *Measurement of the Neutrino Neutral-Current Elastic Differential Cross Section on Mineral Oil at $E_\nu \sim 1$ GeV*, *Phys. Rev.* **D 82** (2010) 092005 [arXiv:1007.4730] [inSPIRE].

[55] Double CHOOZ collaboration, Y. Abe et al., *Reactor electron antineutrino disappearance in the Double CHOOZ experiment*, *Phys. Rev.* **D 86** (2012) 052008 [arXiv:1207.6632] [inSPIRE].

[56] C.T. Kishimoto and G.M. Fuller, *Lepton Number-Driven Sterile Neutrino Production in the Early Universe*, *Phys. Rev.* **D 78** (2008) 023524 [arXiv:0802.3377] [inSPIRE].

[57] L.A. Gilbert, G.M. Fuller and E. Grohs, *Implications of sterile neutrino oscillations on primordial abundances and energy density in the early universe*, in preparation (2015).

[58] A.D. Dolgov, S.H. Hansen, S. Pastor, S.T. Petcov, G.G. Raffelt and G.G. Raffelt, *Cosmological bounds on neutrino degeneracy improved by flavor oscillations*, *Nucl. Phys.* **B 632** (2002) 363 [hep-ph/0201287] [inSPIRE].

[59] J.L. Menestrina and R.J. Scherrer, *Dark Radiation from Particle Decays during Big Bang Nucleosynthesis*, *Phys. Rev.* **D 85** (2012) 047301 [arXiv:1111.0605] [inSPIRE].

[60] E.W. Otten and C. Weinheimer, *Neutrino mass limit from tritium β decay*, *Rept. Prog. Phys.* **71** (2008) 086201 [arXiv:0909.2104] [inSPIRE].

[61] G. Drexlin, *Direct neutrino mass measurements*, *J. Phys. Conf. Ser.* **136** (2008) 022031 [inSPIRE].

[62] A. Kusenko, S. Pascoli and D. Semikoz, *Bounds on heavy sterile neutrinos revisited*, *JHEP* **11** (2005) 028 [hep-ph/0405198] [inSPIRE].

[63] CHARM collaboration, F. Bergsma et al., *A Search for Decays of Heavy Neutrinos*, *Phys. Lett.* **B 128** (1983) 361 [inSPIRE].

[64] G. Bernardi, G. Carugno, J. Chauveau, F. Dicarlo, M. Dris et al., *Search for Neutrino Decay*, *Phys. Lett.* **B 166** (1986) 479 [inSPIRE].

[65] G. Bernardi, G. Carugno, J. Chauveau, F. Dicarlo, M. Dris et al., *Further limits on heavy neutrino couplings*, *Phys. Lett.* **B 203** (1988) 332 [inSPIRE].

[66] S.A. Baranov, Y. Batusov, A.A. Borisov, S.A. Bunyatov, V.Y. Valuev et al., *Search for heavy neutrinos at the IHEP-JINR neutrino detector*, *Phys. Lett.* **B 302** (1993) 336 [inSPIRE].

[67] P. Nédélec, *Tau - sterile neutrino mixing in NOMAD*, *Nucl. Phys. Proc. Suppl.* **98** (2001) 37 [inSPIRE].

[68] S. Mertens, K. Dolde, M. Korzeczek, F. Glueck, S. Groh et al., *Wavelet approach to search for sterile neutrinos in tritium β-decay spectra*, *Phys. Rev.* **D 91** (2015) 042005 [arXiv:1410.7684] [inSPIRE].

[69] A.D. Dolgov, S.H. Hansen, G. Raffelt and D.V. Semikoz, *Heavy sterile neutrinos: Bounds from big bang nucleosynthesis and SN 1987A*, *Nucl. Phys.* **B 590** (2000) 562 [hep-ph/0008138] [inSPIRE].

[70] M. Kaplinghat, L. Knox and Y.-S. Song, *Determining neutrino mass from the CMB alone*, *Phys. Rev. Lett.* **91** (2003) 241301 [astro-ph/0303344] [inSPIRE].

[71] S.H. Hansen and Z. Haiman, *Do we need stars to reionize the universe at high redshifts? Early reionization by decaying heavy sterile neutrinos*, *Astrophys. J.* **600** (2004) 26 [astro-ph/0305126] [inSPIRE].

[72] S. Hannestad and G. Raffelt, *Cosmological mass limits on neutrinos, axions and other light particles*, *JCAP* **04** (2004) 008 [hep-ph/0312154] [inSPIRE].

[73] F. De Bernardis, T.D. Kitching, A. Heavens and A. Melchiorri, *Determining the Neutrino Mass Hierarchy with Cosmology*, *Phys. Rev.* **D 80** (2009) 123509 [arXiv:0907.1917] [inSPIRE].

[74] S. Hannestad, A. Mirizzi, G.G. Raffelt and Y.Y.Y. Wong, *Neutrino and axion hot dark matter bounds after WMAP-7*, *JCAP* **08** (2010) 001 [arXiv:1004.0695] [INSPIRE].

[75] M. Archidiacono, A. Cooray, A. Melchiorri and S. Pandolfi, *CMB Neutrino Mass Bounds and Reionization*, *Phys. Rev.* **D 82** (2010) 087302 [arXiv:1010.5757] [INSPIRE].

[76] E. Giusarma, M. Corsi, M. Archidiacono, R. de Putter, A. Melchiorri et al., *Constraints on massive sterile neutrino species from current and future cosmological data*, *Phys. Rev.* **D 83** (2011) 115023 [arXiv:1102.4774] [INSPIRE].

[77] G.M. Fuller, E. Grohs, C.T. Kishimoto, M.W. Paris and A. Vlasenko, *Energy transport in neutrino decoupling and big bang nucleosynthesis*, in preparation (2015).

[78] M.J. Savage, R.A. Malaney and G.M. Fuller, *Neutrino Oscillations and the Leptonic Charge of the Universe*, *Astrophys. J.* **368** (1991) 1 [INSPIRE].

[79] K.N. Abazajian, J.F. Beacom and N.F. Bell, *Stringent constraints on cosmological neutrino anti-neutrino asymmetries from synchronized flavor transformation*, *Phys. Rev.* **D 66** (2002) 013008 [astro-ph/0203442] [INSPIRE].

[80] Y.Y.Y. Wong, *Analytical treatment of neutrino asymmetry equilibration from flavor oscillations in the early universe*, *Phys. Rev.* **D 66** (2002) 025015 [hep-ph/0203180] [INSPIRE].

[81] G.M. Fuller, W.A. Fowler and M.J. Newman, *Stellar weak interaction rates for intermediate-mass nuclei. IV - Interpolation procedures for rapidly varying lepton capture rates using effective log (ft)-values*, *Astrophys. J.* **293** (1985) 1 [INSPIRE].

[82] E.W. Kolb and M.S. Turner, *The early universe*, *Front. Phys.* **69** (1990).

[83] J.P. Kneller and G. Steigman, *BBN for pedestrians*, *New J. Phys.* **6** (2004) 117 [astro-ph/0406320] [INSPIRE].

[84] J.N. Ariche, G.M. Fuller and E. Grohs, *Coupling lepton numbers and sterile neutrinos to the big bang nucleosynthesis and photon decoupling epochs*, in preparation (2015).

[85] K.N. Abazajian et al., *Neutrino Physics from the Cosmic Microwave Background and Large Scale Structure*, *Astropart. Phys.* **63** (2015) 66 [arXiv:1309.5383] [INSPIRE].